HHS Public Access

Author manuscript

Sci Immunol. Author manuscript; available in PMC 2023 November 12.

Published in final edited form as:

Sci Immunol. 2023 May 12; 8(83): eabq7486. doi:10.1126/sciimmunol.abq7486.

Transcriptional programming of CD4+ T_{RM} differentiation in viral infection balances effector- and memory-associated gene expression

Quynh P Nguyen[1,#], **Kennidy K Takehara**[1,#], **Tianda Z Deng**[1], **Shannon O'Shea**[1], **Maximilian Heeg**[1], **Kyla D Omilusik**[1], **J Justin Milner**[1], **Sara Quon**[1], **Matthew E Pipkin**[2], **Jinyong Choi**[3,4], **Shane Crotty**[4,5], **Ananda W Goldrath**[1,*]

[1]School of Biological Sciences, Department of Molecular Biology, University of California, San Diego, La Jolla, CA

[2]Department of Immunology and Microbiology, The Scripps Research Institute, Jupiter, Florida

[3]Department of Microbiology, College of Medicine, The Catholic University of Korea

[4]Center for Infectious Disease and Vaccine Research, La Jolla Institute for Immunology, La Jolla, CA

[5]Division of Infectious Diseases, Department of Medicine, University of California, San Diego, La Jolla, CA

Abstract

Following resolution of infection, T cells differentiate into long-lived memory cells that recirculate through secondary lymphoid organs or establish residence in tissues. In contrast to $CD8^+$ tissue-resident memory T cells (T_{RM}), the developmental origins and transcriptional regulation of $CD4^+$ T_{RM} remain largely undefined. Here, we investigated the phenotypic, functional, and transcriptional profiles of $CD4^+$ T_{RM} in the small intestine (SI) responding to acute viral infection, revealing a shared gene-expression program and chromatin accessibility profile with circulating T_H1 cells and the progressive acquisition of a mature T_{RM} program. Single-cell RNA-sequencing identified heterogeneity among established $CD4^+$ T_{RM} which were predominantly located in the lamina propria, as well as revealing a population of cells that co-expressed both effector- and memory-associated genes, including the transcriptional regulators Blimp1, Id2, and Bcl6. T_H1-associated Blimp1 and Id2 and T_{FH}-associated Bcl6 were required for early T_{RM} formation and development of a mature T_{RM} population in the SI. These results demonstrate a developmental relationship between T_H1 effector cells and the establishment of early T_{RM}, as well as highlighting

*Correspondence should be addressed to agoldrath@ucsd.edu, Ananda Goldrath, University of California, San Diego, 9500 Gilman Drive 0377, La Jolla, CA 92093.

Author Contributions

Q.P.N. conceived of the study, designed and performed experiments, analyzed and interpreted the data, and wrote the manuscript. K.T. designed and performed experiments, analyzed and interpreted the data, and edited the manuscript. T.D., S.O., K.O., J.M., and S.Q. performed experiments and contributed ideas. M.H. performed computation analysis. J.C. and S.C contributed valuable mice, experimental ideas, and key edits for this manuscript. M.P. designed experiment reagents and contributed experimental ideas and key edits for this manuscript. A.W.G. conceived the study, interpreted data, and wrote the manuscript.

#These authors contributed equally to this work.

differences in $CD4^+$ versus $CD8^+$ T_{RM} populations, providing insights into the mechanisms underlying the origins, differentiation, and persistence of $CD4^+$ T_{RM} in response to viral infection.

One sentence summary

Maintenance of anti-viral $CD4^+$ T_{RM} relies on transcriptional regulators that program both T_H1 and T_{FH} populations.

Introduction

In response to infection, $CD4^+$ T cells differentiate into diverse effector cell subsets reflecting the infection milieu, including type 1-helper T cells (T_H1), type 2-helper T cells (T_H2), T helper 17 cells (T_H17), regulatory T cells (T_{REG}) and follicular helper cells (T_{FH}) (1). After pathogen clearance, a portion of the responding cells persists in secondary lymphoid organs (SLOs) or tissues as long-lived $CD4^+$ tissue-resident memory T cells (T_{RM}) (2) with heterogenous phenotype, function, and trafficking properties (3–6). The T_{FH} subset, which migrates to germinal centers (GC) and mediates B-cell antibody responses, is the predominant memory population, exhibits greater multipotency in response to pathogen rechallenge, and includes precursors of recirculating $CD4^+$ memory T cells (4, 7, 8).

Long-lived $CD4^+$ T_{RM} cells are found in most tissues including lung, skin, female reproductive tract (FRT), and small intestine (SI) (9, 10); these cells are critical for recruiting innate immune cells, $CD8^+$ T cells, and B cells to sites of reinfection (11). While the phenotype, function, and regulation of $CD4^+$ T_{RM} differ among infection models and tissue types, $CD4^+$ T_{RM} generally express high levels of CD69, physically cluster and interact with other immune cell populations to optimize function, and require tissue-specific cytokines for their recruitment and maintenance (9). Lung $CD4^+$ T_{RM} play a critical role against bacterial, viral, worm infections and in allergic asthma (12), while skin $CD4^+$ T_{RM} cells mediate response to herpes simplex virus (HSV) and *Leishmania major* infection (13, 14). Intravaginal HSV-specific $CD69^+$ $CD4^+$ T_{RM} localize in clusters containing $CD8^+$ T cells, macrophages, and other antigen-presenting cells, and produce interferon-gamma (IFNγ) to directly inhibit viral replication (15). Defining the developmental origins of $CD4^+$ T_{RM} has proved challenging due to heterogeneity within the effector T cell population and unresolved mechanisms of $CD4^+$ memory T cell differentiation (9). $CD4^+$ T_{RM} have been developmentally linked to T_H cell subsets with characteristics of the relevant helper effector cells, such as intestinal T_H1 cells in *Listeria* infection, lung T_H2 cells in allergic asthma, and lung T_H17 cells in *Klebsiella pneumonia* immunization (16–19). This raises the question of whether there is a true T_{RM} precursor, or whether T_{RM} cells are long-lived effector T cells lodged in tissues.

The expression and activity of transcriptional regulators critical in circulating $CD4^+$ T cell differentiation, such as Blimp1 and Bcl6, are not well characterized in the context of $CD4^+$ T_{RM} population. Bcl6 promotes T_{FH} and memory $CD4^+$ T cell populations by inhibiting Blimp1, while Blimp1 promotes T_H1 differentiation by directly inhibiting Bcl6 and T_{FH} development (4, 20). Bcl6-deficient $CD4^+$ T cells following influenza infection did not differentiate into lung T resident helper (T_{RH}) cells, whereas loss of Bcl6 in effector $CD4^+$

T cells following house dust mite exposure resulted in more $CD4^+$ T cells in the lung, highlighting the involvement of Bcl6 in $CD4^+$ T_{RM} differentiation (19, 21, 22). Notably, Bcl6 and Blimp1 are co-expressed by regulatory follicular helper cells (T_{FR}), a population that displays hybrid functions of T_{REG} and T_{FH} (23, 24). $CD8^+$ T_{RM}, which also provide protection in non-lymphoid tissues (NLT), upregulate transcriptional programs in common with T_{FH} cells, supporting the idea that $CD4^+$ T_{RM} are related to T_{FH} (25). To facilitate retention in their respective tissues (GCs or NLT) and prevent egress, memory T_{FH} and $CD8^+$ T_{RM} cells express the C-type lectin CD69 (10, 26) and downregulate transcription factor (TF) Kruppel-like factor 2 (Klf2) (27, 28) and its downstream target, egress factor sphingosine-1-phosphate receptor 1 (S1pr1). Furthermore, both T_{FH} and $CD8^+$ T_{RM} subsets express ICOS, thought to induce downregulation of Klf2 (29–31), and Bcl6, which promotes $CD8^+$ T cell memory (20, 32). Conversely, T_H1-associated TFs, Blimp1 (33, 34) and Runx3 (35), are central regulators of the $CD8^+$ T_{RM} program (10, 36). Blimp1 and related TF Hobit cooperate to repress tissue egress genes and maintain HSV-specific $CD8^+$ T_{RM} in the skin (37). Runx3 is expressed at low levels by $CD4^+$ IEL (38), and overexpression of Runx3 in $CD4^+$ T cells mediated TGF-β responsiveness and enhanced $CD8^+$ T cell-like epithelial residency of $CD4^+$ T_{RM} (36). Thus, it is unclear whether $CD4^+$ T_{RM} share a developmental relationship with effector T_H subsets or T_{FH} cells.

E protein TFs and their inhibitors, Id proteins, also play critical regulatory functions in $CD4^+$ T cell differentiation. Id2 is highly expressed by $CD4^+$ T_H1 cells and mediates T_H1 differentiation (39); conversely, Id3 is important for T_{FH} development (40). Importantly, Bcl6 can directly inhibit Id2 expression, allowing E protein-driven expression of CXC-chemokine receptor type 5 (CXCR5) by T_{FH} cells (39). In acute LCMV infection, Id3 expression also marks long-lived $CD4^+$ memory T cells in circulation (41). Despite these TFs being vital in development of circulating $CD4^+$ T cell subsets, it is unclear how they influence the T_{RM} population in viral infection.

Here we studied the immune response to acute infection with Lymphocytic Choriomeningitis Virus-Armstrong (LCMV-Arm), focusing on key transcriptional regulators of $CD4^+$ T_H differentiation, tissue-residency, and homeostasis. $CD4^+$ T_{RM} exhibited an effector-like identity, with cell-surface molecule expression, cytokine production, and enrichment of the T_H1 gene-expression signature. In contrast to $CD8^+$ T_{RM}, $CD4^+$ T_{RM} did not express CD103, accumulated in the lamina propria (LP) rather than the epithelium, showed delayed progressive acquisition of the mature T_{RM} program, and did not require Runx3 for their development. Notably, single-cell RNA sequencing demonstrated that the LP $CD4^+$ T_{RM} population at a memory timepoint displayed heterogeneity, and a portion of cells co-expressed the T_H1 and T_{FH} lineage-defining transcriptional antagonists, Blimp1 and Bcl6. Finally, Blimp1, Id2, and Bcl6 were all ultimately required for establishment of $CD4^+$ T_{RM} in response to viral infection.

Results

Antiviral CD4$^+$ T_{RM} share phenotypic, transcriptional, and epigenetic profiles with circulating T_H1 cells

To better understand the developmental origins of antiviral CD4$^+$ T_{RM}, specifically how T_{RM} relate to effector CD4$^+$ T_H subsets in SLOs, we examined the CD4$^+$ T cell response to acute LCMV infection. SMARTA TCR transgenic CD4$^+$ T cells specific for LCMV were transferred into CD45$^+$ congenically distinct host mice that were subsequently infected with LCMV-Arm. Following infection, SMARTA T cells in specified tissues were phenotyped by flow cytometry: spleen (SPL), mesenteric lymph nodes (mLN), both the epithelium (IEL) and the lamina propria (LPL) of the small intestine (SI), kidneys (KID), liver (LIV), and lungs for (Fig. 1A & fig. S1A–D). To distinguish between cells in the vasculature (IV$^+$) and tissues (IV$^-$), mice were injected with an anti-Thy1 antibody prior to tissue harvest and IV$^-$ cells were studied. Circulating CD4$^+$ effector T cell subsets were characterized by cell-surface molecules: T_H1 cells by expression of SLAM, and T_{FH} cells by expression of CXCR5 (1). SMARTA CD4$^+$ T cells in the spleen and mLN showed substantial populations of both T_H1 cells and T_{FH} cells, with a higher frequency of T_{FH} cells present on days 21 and 40 (Fig. 1B,C & fig. S1C,E). Interestingly, the lung population included a sizable portion of CXCR5$^+$ cells, consistent with a previously described T_{FR} population in influenza infection (23). However, CD4$^+$ T cells across all tissues and T_H1 cells in the spleen and mLN were predominantly SLAM$^+$ CXCR5$^-$ at days 7, 21, and 40, supporting a direct relationship between T_{RM} and T_H1 subsets.

CD4$^+$ T_{RM} were next analysed for expression of molecules associated with tissue-residency and memory T cells, revealing both shared characteristics and notable differences with circulating T_H cells. CD8$^+$ T_{RM} can be distinguished from the circulating memory populations by their expression of the C-type lectin CD69 and the integrin CD103 (27, 42). However, the majority of CD4$^+$ T_{RM} in IEL and LPL expressed CD69 but not CD103 at all timepoints (Fig. 1D,E & fig. S1F), consistent with previous studies (11). There was a lower frequency of IV$^-$ cells in the kidneys, liver, and lungs which expressed CD69, indicating tissue-specific requirements for residency (Fig. S1F). CD27 has been shown to be critical in memory T cell development (43) and marks memory human CD4$^+$ T cell subsets with high CD27 expression associated with less antigen recall ability and greater plasticity (44, 45). At the peak response to LCMV-Arm infection, circulating and SI SMARTA T cells were predominantly CD27$^+$ (Fig. 1D,E). By day 21 of infection, the majority of spleen and mLN CD4$^+$ T cells remained CD27$^+$, while approximately half of the IEL and LPL cells were CD27$^-$. Lymphocyte antigen 6 complex (Ly6C) marks CD4$^+$ memory T cells, where terminally differentiated cells are Ly6C$^+$ and multi-potent cells are Ly6C$^-$ (5, 46). At the peak of infection, approximately 50% of CD4$^+$ T cells in the spleen, mLN and SI expressed Ly6C (Fig. 1D,E). However, by day 21, the majority of SI CD4$^+$ T_{RM} were Ly6C$^-$, while the frequencies in circulating populations remained stable consistent with previous studies (11, 18). Thus, CD4$^+$ T cells in tissues could be distinguished from their circulating counterparts by elevated CD69 expression, loss of Ly6C expression, and heterogeneous CD27 expression.

To determine whether the $CD4^+$ T_{RM} response differed with different antigens, we utilized LCMV-Arm specific NIP mice (47). NIP cells have been shown to efficiently induce NP-specific GC B cells and generate greater numbers of T_{FH} during infection, relative to GP-specific SMARTA cells (47). We also analyzed $GP_{66–77}$-I-A^b tetramer $CD4^+$ T cells to assess endogenous $CD4^+$ T cell responses. We found that NIP and tetramer$^+$ $CD4^+$ T cells in the SI also showed a bias towards the T_H1 phenotype and expressed CD69, similar to SMARTA T cells (Fig. S1G, H).

Global gene expression by SI $CD4^+$ T_{RM} cells was compared to effector T_H subsets, SMARTA $SLAM^+$ T_H1 cells, $CXCR5^+$ T_{FH} cells, and SI T_{RM} at days 7 and 21 after infection by bulk RNA sequencing. Principal component analysis (PCA) of gene expression revealed a clear separation of D21 IEL/LPL samples from all other samples (Fig. 2A). Day 7 IEL and LPL $CD4^+$ T cells aggregated closely with day 7 T_H1 cells, consistent with their phenotypic similarities. We also observed some separation between D21 IEL and LPL samples, perhaps due to heterogeneity driven by tissue localization or functional requirements. Gene enrichment analysis (GSEA) was used to compare the transcriptional profiles of $CD4^+$ T cells from the SI and spleen on day 21 of infection (Fig. 2B). SI $CD4^+$ T_{RM} cells were significantly enriched for the T_H1 gene-expression signature (7) with minimal enrichment of the T_{FH} signature (7). Furthermore, $CD4^+$ T_{RM} were enriched for published gene-expression signatures of both $CD8^+$ T_{RM} (48) and $CD4^+$ non-lymphoid tissue (NLT) (11) when compared to both T_H1 or T_{FH} splenic subsets (Fig. 2B). This indicates that $CD4^+$ T_{RM} at, an early memory time point had upregulated the tissue-residency program expressed by late memory T_{RM}. We next assessed the expression of specific genes encoding surface receptors, effector molecules, and TFs with known roles in effector and memory $CD4^+$ T cell development or the $CD8^+$ T_{RM} program (Fig. 2C). Compared to naive $CD4^+$ T cells, IEL and LPL effector and memory populations expressed genes associated with SI-homing such as *Ccr9* and revealed expression consistent with the T_{RM} program including expression of *Cd69* and loss of *Klf2* and *S1pr1*. $CD4^+$ T_{RM} cells in the IEL and LPL at day 21 expressed genes associated with both the effector/T_H1 program, such as *Gzma*, *Gzmb*, *Ifng*, *Tbx21*, *Prdm1*, *Id2*, *Stat4* and the memory/T_{FH} identity such as *Icos*, *Pdcd1*, *Stat3, Bcl6*. Notably, D21 SI and T_H1 populations expressed both *Bcl6* and *Prdm1* concurrently, as these TFs are known reciprocal antagonists.

We performed Assay for Transposase-Accessible Chromatin sequencing (ATACseq) to assess accessible regulatory regions in these $CD4^+$ T cell populations. A correlation heatmap comparing differentially accessible regions (DARs) among all samples revealed that D7 IEL cells were more closely associated with the T_H1 subset at both effector and memory time points (Fig. 2D). We directly quantified peaks in differentially accessible regions for D7 IEL, T_{FH}, or T_H1 cells and found few peaks distinguishing IEL and T_H1 samples compared to 2,036 DARs between the IEL and T_{FH} subset (Fig. 2E,F). Of the DAR-associated genes, more were differentially expressed genes between IEL and T_{FH} populations compared to IEL and T_H1 cells (Fig. 2F), in a pattern consistent with correlated accessibility and expression. When we compared specific gene loci among different time points and tissues, we observed similar profiles for D7 IEL and D7 T_H1 cells, which were distinct from naive and D7 T_{FH} profiles (Fig. 2G). Overall, these data revealed the acquisition of T_{RM} features in response to LCMV-Arm as well as similarities between $CD4^+$ T_{RM} and effector T_H1 cells

in surface-receptor expression, transcriptional profile, and chromatin landscape, suggesting that these two populations are related.

Antiviral T_H1 $CD4^+$ T cells show tissue migration potential and produce T_H1 cytokines

We further investigated the differentiation and function of circulating and SI-residing $CD4^+$ T cells during infection. We profiled CCR9 and CD49d expression of C-C chemokine receptor type 9 (CCR9) and integrin alpha 4 (CD49d), which mediate gut-homing and are upregulated by cells that traffic to the SI (49) (Fig. 3A,B). The proportion of $CCR9^+CD49d^+$ $CD4^+$ T cells increased in the IEL and LPL as cells migrated in to the tissue. Interestingly, of the $CCR9^+CD49d^+$ cells with the potential to traffic to the SI, more than 80% of cells from the spleen and 90% of cells from the mLN were $SLAM^+$ T_H1 effector cells (Fig. 3C,D), raising the possibility of a developmental relationship between circulating T_H1 cells and SI $CD4^+$ T_{RM}. While a number of T_{FH} cells express CCR9 at day 6 of infection and therefore can access SI tissues, there gut-homing cells were biased towards the T_H1 phenotype (Fig. 3C). Recently, two subsets of influenza-specific resident $CD4^+$ T cells in the lung were described: $T_{RM}1$ cells with a T_H1 phenotype expressing P-selectin glycoprotein ligand-1 (PSGL1), and T_{RH} cells with a T_{FH} phenotype expressing folate receptor 4 (FR4) (21, 22). In our studies, SI $CD4^+$ T_{RM} populations were $PSGL1^+$ and did not express FR4 (fig. S2A), suggesting the type of infection and tissue-specific cues may direct the differentiation of distinct $CD4^+$ T_{RM} subsets in the lung versus SI.

To assess the functional capacity of anti-viral SI $CD4^+$ T_{RM} and splenic effector T cell subsets, SMARTA $CD4^+$ T cells from each tissue were re-stimulated *ex vivo* with the $GP_{61–80}$ peptide and production of IFNγ and TNFα was quantified (Fig. 3E). An increased proportion of $CD4^+$ T cells in the SI produced both cytokines compared to those in the spleen on day 7 of infection; however, the frequency of cytokine-producing cells in the SI was lower than splenic T cells at a memory time point. SI $CD4^+$ T cells also expressed higher levels of Granzyme A and B at both effector and memory time points compared to $CD4^+$ T cells from the spleen and mLN (Fig. 3F). A cytotoxic subset of $CD4^+$ T cells, T_HCTL, has been shown to develop in the lung following influenza A infection (50) and mediate MHC-II-restricted cytotoxicity, produce high levels of effector cytokines, and uniquely express inhibitory molecules NKG2A/C/E (51). To determine if there were parallels between T_HCTL and T_{RM} in viral infection beyond granzyme expression, we evaluated expression of NKG2A/C/E by LCMV-specific $CD4^+$ T_{RM} compared to circulating $CD4^+$ T cells, $CD8^+$ T cells, and NK cells on day 21 of infection. $CD4^+$ SMARTA T cells in both SI compartments expressed minimal levels of NKG2A/C/E compared to circulating SMARTA T cells, $CD8^+$ T cells, and NK cells (fig. S2B). Despite their shared expression of IFNγ and Granzyme B, SI-resident $CD4^+$ T_{RM} cells did not express canonical markers of T_HCTL, which further indicated that the T_{RM} program may be influenced by infection type and tissue-specific cues. These data overall highlighted similarities between $CD4^+$ T_{RM} and T_H1 effector cells.

$CD4^+$ T cells show delayed progressive acquisition of the mature T_{RM} signature

PCA analysis of bulk RNAseq data revealed separation of SI populations at days 7 and 21, suggesting additional maturation from the effector to the mature T_{RM} population (Fig. 2A).

Comparison of SI and splenic T cells showed that D7 T_{RM} cells expressed 13–15% of the genes from the mature D21 T_{RM} and had not upregulated the $CD4^+$ NLT gene signature (Fig. 4A,B). Interestingly, the kinetics of $CD4^+$ and $CD8^+$ T_{RM} maturation appear to be different: effector $CD8^+$ T cells in the SI on day 7 of infection have already acquired the majority of the mature $CD8^+$ T_{RM} expression pattern at day 35, with 57% of "core" T_{RM} genes shared between the two time points (fig. S3A and (48)). Tissue localization may play a role in the kinetics of T_{RM} maturation, as we observed more $CD4^+$ T_{RM} cells in the lamina propria at day 21 of infection, compared to $CD8^+$ T_{RM} cells, which localized to the epithelium (fig. S3B). Differential localization by $CD4^+$ T_{RM} for HSV-specific responses in the skin has been observed where memory $CD4^+$ T_{RM} accumulate in the dermis and $CD8^+$ T_{RM} localize to the epidermis (10). Thus, acquisition of the full $CD4^+$ T_{RM} gene-expression program requires more time than the $CD8^+$ T_{RM} program.

To explore differences in the transcriptional programs between effector and memory SI $CD4^+$ T cell subsets and to evaluate heterogeneity of cells within these populations, we utilized bulk RNAseq and single-cell RNAseq (scRNAseq) to compare gene expression. Due to the cell number limitations we were only able to generate LPL samples for scRNAseq at the memory time point. Unsupervised Uniform Manifold Approximation and Projection (UMAP) clustering separated samples by tissues, with D21 LPL cells (purple), and D21 SPL cells (dark blue) grouped separately from other samples and enriched for their respective gut or spleen gene-expression signatures generated from our bulk RNAseq (Fig. 4C). While a subset of D7 IEL and LPL cells (yellow, red) clustered together, a high proportion of D7 SI cells were intermixed with D7 SPL cells (green) and were observed throughout the UMAP. Utilizing our bulk RNAseq data and published datasets (11, 48), we evaluated the expression of the spleen and SI gene signatures for single-cell samples (Fig. 4C,D). While D21 spleen and LPL samples were enriched for the respective spleen or SI gene signatures, clusters dominated by D7 cells expressed low to intermediate levels of both gene signatures, suggesting that cells at day 7 were not yet defined by a specific program (Fig. 4C,D). The memory T_H1 gene signature (>1.5 fold-change between D41 and D7 T_H1 cells) was enriched in both the D7 and D21 SI clusters compared to splenic cells, although the D7 spleen replicates did show variable expression. The memory T_{FH} gene signature (>1.5 fold-change between D41 and D7 T_{FH} cells) was only enriched in the D21 SPL samples, once again highlighting the T_H1 versus T_{FH} division among spleen $CD4^+$ T cells (Fig. 4D). The D21 LPL cluster showed highest enrichment of the $CD4^+$ NLT and $CD8^+$ T_{RM} gene signature, with moderate expression of residency-related genes by D7 SI samples, consistent with the observation that D7 SI $CD4^+$ T cells undergo additional maturation.

Focused analysis of spleen and SI $CD4^+$ T cells from day 7 of infection revealed 7 clusters, with all clusters containing a mixture of cells from both spleen and SI (fig. S4A). The clusters were separated into T_H1 and T_{FH} subsets, with clusters 2, 3, 4, 5, and 6 enriched for the effector T_H1 gene signature, including *Slamf1 and Id2*, while clusters 0, 1, and 5 were enriched for the effector T_{FH} gene signature, including *Cxcr5* and *Id3* (Fig. S4B,C). The CD4 NLT (11) gene signature was also enriched in clusters 2, 3, 4, 5, and 6 with accompanying expression of tissue-associated genes such as *Cd69* and *Ccr9*. Interestingly, cells in clusters 2, 4, and 5 expressed both T_{FH} and T_H1 gene-expression signatures, consistent with the notion that SI $CD4^+$ T cells at day 7 of infection are still differentiating

and likely require further cues for their full maturation into CD4$^+$ T_{RM}. RNA velocity analysis on scRNA-seq samples was used to assess potential developmental trajectories for CD4$^+$ T_{RM} cells (Fig. 4E and fig S4D). This revealed a general progression of D7 splenic CD4$^+$ T cells towards D7 IEL and LPL populations, evolution into the mature T_{RM} D21 LPL population (Fig. 4F and fig. S4E), and a gradual increase in expression of the memory T_H1 gene signature between days 7 and 21 (Fig. 4G). Overall, our sequencing data highlighted differences between effector and memory SI CD4$^+$ T cells, with D7 SI T cells sharing transcriptional similarities with D7 splenic T cells and the evolution to a distinct tissue-resident population by D21 post infection.

CD4$^+$ T_{RM} exhibit heterogeneity and express effector and memory-associated genes

To examine heterogeneity of established CD4$^+$ T_{RM}, we analyzed scRNAseq data focusing on D21 spleen and LPL CD4$^+$ T cells (Fig. 5A). The LPL clusters showed enrichment for the CD4$^+$ NLT (11), CD8$^+$ T_{RM} (48), and memory T_H1 gene signatures, while cells in the spleen expressed the highest level of the memory T_{FH} gene signature compared with LPL cells (Fig. 5B). Gene signature enrichment analysis of the LPL cells revealed some heterogeneity among cells in the LPL population, with differential expression of of T_{RM}-associated genes (Fig. 5C). We next focused on expression of TFs involved in the effector versus memory programs, specifically *Id2* and *Prdm1* for T_H1 effector cells and *Bcl6* and *Stat3* for memory T cells (52) (Fig. 5D); all four genes showed elevated expression by the LPL compared to spleen. Unlike the SI CD8$^+$ T_{RM} population, which contains distinct subsets marked by Id3 and Blimp1, *Id3* expression was not deteted in scRNAseq of D21 LPL cells or bulk RNAseq of the total SI population (Fig. 5D). We also observed differential expression of *Cd27* and *Cd69* mRNA, consistent with flow cytometry data (Fig. 2C). Finally, we examined expression of *Runx3* and *Klf2*, which regulate CD8$^+$ T_{RM} development (27, 48). LPL cells were enriched for *Runx3* but expressed low levels of *Klf2* compared to the spleen CD4$^+$ T cells, with accompanying downregulation of its target *S1pr1* (Fig. 5D). These data suggested that mechanisms of tissue retention are shared by both CD4$^+$ and CD8$^+$ T_{RM}.

Expression of both *Blimp1* and *Bcl6*, typically considered reciprocal antagonists, by T_{RM} at levels higher than splenic CD4$^+$ T cell populations in bulk RNAseq analysis was unexpected (Fig. 2C). We compared expression of either *Bcl6* and *Prdm1* or *Stat3* and *Stat4* (which are associated with memory and effector fates, respectively) in single cells (Fig. 5E). A number of cells co-expressed the TF pair, *Bcl6* and *Prdm1*, as well as *Stat3* and *Stat4*, suggesting that CD4$^+$ T_{RM} have a hybrid transcriptional program that drives aspects of both effector and memory gene-expression programs. To confirm these findings, we transferred Blimp1-YFP SMARTA CD4$^+$ T cells to congenically distinct mice that were subsequently infected with LCMV-Arm. On day 14 of infection, Blimp1$^+$ and Blimp1$^-$ SMARTA T cells from the spleen and SI were sorted and *Bcl6* mRNA levels were compared using qPCR. We observed a two to three-fold increase in *Bcl6* mRNA in Blimp1-YFP$^+$ IEL and LPL cells compared to splenic populations, confirming co-expression of *Blimp1* and *Bcl6* (Fig. 5F). Together, these data highlighted the heterogeneity within the SI CD4$^+$ T cell population that begins during the effector phase, and implicated Blimp1, Id2, and Bcl6 as regulators of a CD4$^+$ T_{RM}

residency program, allowing for sustained effector functions and persistence as long-lived memory T cells.

Blimp1 and Id2 are required for virus-specific CD4$^+$ T_{RM} progenitor cells in the SI

To evaluate the relationship between early CD4$^+$ T_{RM} and T_H1 populations, we investigated the role of Blimp1 and Id2, TFs in T_H1 development and effector function (20, 39). D7 and D21 SI T_{RM} expressed both factors, suggesting that Blimp1 and Id2 may function in the seeding or development of CD4$^+$ T_{RM} (Fig. 2C, 5D). Importantly using PageRank analysis (53) of RNAseq and ATACseq samples, Blimp1 was also predicted as a regulator of gene expression by SI CD4$^+$ T cell samples relative to splenic T cells at day 7 of infection (fig. S5A). Additionally, PageRank also predicted *Tcf12*, encoding the E protein transcription factor HEB and target of Id2 inhibition, as regulator of SI CD4$^+$ T cells. These data suggested that T_H1-associated Blimp1 and Id2 may be critical factors in early T_{RM} development.

To gain insight into the kinetics of Blimp1 expression by circulating and SI CD4$^+$ T cells following viral infection, Blimp1-YFP SMARTA CD4$^+$ T cells were studied (Fig. 6A,B). On day 7 of infection, the majority of SI CD4$^+$ T cells expressed Blimp1 compared to only 40–50% Blimp1$^+$ CD4$^+$ T cells in the circulation. By day 21 of infection, the frequency of Blimp1$^+$ CD4$^+$ T cells in the SI decreased to approximately 60%, but was still higher than in circulating CD4$^+$ T cell population. To determine if Blimp1 contributes to CD4$^+$ T_{RM} differentiation, we transferred *Blimp1*$^{f/f}$*CD4-Cre*$^+$ SMARTA T cells (Blimp1-KO) as a 50:50 mix with wild-type SMARTA T cells (WT) into congenically distinct hosts and and the frequency and number of WT to Blimp1-KO cells were compared over the course of infection (Fig. 6C,D and fig. S5B). Loss of Blimp1 significantly impaired the accumulation of early CD4$^+$ T_{RM} at day 7 in all tissues, particularly the SI IEL and LPL, with Blimp1-KO CD4$^+$ T cells making up ~10–15 % of the total SMARTA population isolated from the SI. As a control, a 50:50 mix of CD4-Cre$^+$ and WT CD4-Cre$^-$ SMARTA cells was followed as well; on day 7 of infection the ratio of Cre$^+$ and Cre$^-$ cells showed that Cre expression did not impair the accumulation of cells compared to wildtype cells (Fig. S5C). There was no evidence of delayed T_{RM} differentiation as the Blimp1-KO SMARTA CD4$^+$ T cells remained at a dramatically reduced proportion compared to WT cells at the memory time points (Fig. 6C,D and fig. S5C). Despite an absence of SLAM$^+$ T_H1 cells at day 7 (Fig. S5D), there was a similar frequency of WT and Blimp1-KO SMARTA cells in the spleen; however, by day 14 of infection, the proportion of Blimp1-KO CD4$^+$ T cells was reduced compared to WT cells in the spleen and mLN (Fig. 6C,D and fig. S5C). Cell numbers reflected the frequencies, with significantly fewer Blimp1-KO compared to WT CD4$^+$ T cells in the SI by day 7 of infection (Fig. S5E,F). Given the critical role of Blimp1 in T_H1 differentiation, we specifically compared the WT and KO frequencies within the T_H1 population. The deficit of Blimp1-KO CD4$^+$ T cells was significantly different between the SI and mLN and the IEL and spleen when comparing the frequency of KO to WT cells (fig. S5G). Expression of gut-homing markers CCR9 and CD49d on WT and Blimp1-KO cells was significantly reduced on KO cells in both the circulation and SI (Fig. S5H), suggesting Blimp1 both promotes the ability of effector CD4$^+$ T cells to migrate into the SI and supports T_H1 differentiation. We also examined the effect of Blimp1 deficiency on

$CD4^+$ T_{RM} populations in other mucosal barrier surfaces, including the liver, kidney, and lung (fig. S5I), and observed a 4-fold loss in accumulation of Blimp1-KO cells compared to WT. While Blimp1 has been shown to work in conjunction with the TF Hobit (encoded by *Zfp683)* to mediate T_{RM} development (37, 54), it was not detected in our bulk RNAseq data, and minimally in our scRNAseq datasets. Collectively, these data show that in the absence of T_H1 cells due to the loss of Blimp1 resulted in a failure to accumulate early $CD4^+$ T_{RM} progenitors in the tissues, consistent with T_H1 cells seeding the T_{RM} compartment.

Next, we examined the expression of E protein TF inhibitors Id2 and Id3 by $CD4^+$ T cells in a viral infection, given the prediction of E protein activity in $CD4^+$ T_{RM} by PageRank, the importance of Id2 in T_H1 development (39), and the role of Id3 in memory T cells (41). SMARTA $CD4^+$ T cells expressing Id2-YFP and Id3-GFP reporter alleles (39) were transferred to naive recipients that were subsequently infected with LCMV-Arm. IEL and LPL $CD4^+$ T cells expressed only Id2 at effector and memory time points while a subset of circulating $CD4^+$ T cells expressed both Id2 and Id3 (Fig. 6E,F). Given recent observations that Blimp1 and Id3 expression can identify functionally and transcriptionally distinct subsets in $CD8^+$ T_{RM} and tumor-infiltrating lymphocytes (TIL) (55), we investigated whether similar subsets can be identified in SI $CD4^+$ T_{RM} population using a mouse model expressing both Blimp1-YFP and Id3-GFP reporter alleles (fig. S6A,B). Distinct Blimp1-YFP^+ and Id3-GFP^+ populations in the spleen and mLN were observed while SI $CD4^+$ T cells were mainly $Blimp1^+$, consistent with bulk RNAseq data where T_H1 and SI $CD4^+$ T cells expressed *Id2* and *Prdm1* mRNA while only T_{FH} expressed *Id3* mRNA (Fig. 2C).

We next followed the response of WT and *Id2*$^{f/f}$*CD4-Cre*$^+$ (Id2-KO) SMARTA cells to LCMV-Arm. On day 7 of infection, Id2-KO cells were significantly reduced compared to WT cells in the spleen, mLN, and SI tissues, and SI Id2-KO $CD4^+$ T cells were further reduced compared to spleen and mLN at later time points (Fig. 6G,H and fig. S6C). Consistent with the role of Id2 in T_H1 differentiation, there were fewer Id2-KO $SLAM^+$ T_H1 cells compared to WT on day 7 of infection, and the T_H1 population was absent by day 21 of infection (fig. S6D). The reduction in Id2-KO $CD4^+$ T cells was also reflected in cell numbers (Fig. S6E,F). However, when we compared the frequencies of Id2-KO to WT T_H1 cells, we only observed a significant difference between cells in the spleen and LPL at day 7 of infection (Fig. S6G). The similar deficit in Id2-KO T_H1 cells across all tissues suggests that the impact of Id2 on $CD4^+$ T_{RM} is not SI-specific and associated with the role of this TF in T_H1 differentiation.

Given the phenotypic, transcriptional, and functional similarities between T_H1 and $CD4^+$ T_{RM} cells and the involvement of T_H1-associated TFs in $CD4^+$ T_{RM} development, we hypothesized that the effector T_H1 population contained progenitors of $CD4^+$ T_{RM}. We transferred naive SMARTA $CD4^+$ T cells into congenically distinct hosts and infected the mice with LCMV-Arm. On day 6 of infection, T_H1 and T_{FH} SMARTA T cell populations from the mLN were sorted and re-transferred subset into new recipients ($3.5–6.5\times10^5$ T_H1 or $1–3.5\times10^5$ T_{FH} cells per mouse), which had been infected with LCMV-Arm 3 days prior to transfer. On day 5 following re-transfer, we re-isolated SMARTA cells from the spleen, mLN, and SI and compared the number of recovered cells to the number of transferred cells (Fig. 6I). Consistent with the idea that circulating T_H1 cells give rise to small intestine T_{RM},

we observed a higher ratio of recovered to transferred T_H1 cells in the IEL and LPL samples compared to the transfers of T_{FH} cells. Conversely in the spleen and mLN, there was a higher ratio of recovered to transferred T_{FH} cells. Overall, these data support our hypothesis that $CD4^+$ T_{RM} are developmentally and transcriptionally similar to the circulating T_H1 population.

Bcl6 plays a dual role in the antiviral $CD4^+$ T_{RM} differentiation program

The requirement for Blimp1 and Id2 in early $CD4^+$ T cell accumulation in tissues suggests a relationship between $CD4^+$ T_{RM} and circulating effector T_H1 rather than T_{FH} cells. However, T_{FH} have been posited to share transcriptional programming with $CD4^+$ memory T cells and $CD8^+$ T_{RM}, and we observed expression of *Bcl6* by D21 SI $CD4^+$ T_{RM} (Fig. 2C), which was unexpected given the direct repression of Blimp1 and Id2 expression by Bcl6. To examine if Bcl6 may also be regulating the $CD4^+$ T_{RM} program through a mechanism distinct from its known function within circulating effector and T_{FH} populations, we transferred a 50:50 mix of WT and *Bcl6*$^{f/f}$*CD4-Cre*$^+$ (Bcl6-KO) SMARTA cells into recipients infected with LCMV-Arm (Fig. 7A). Over the course of infection, the frequency and numbers of WT and Bcl6-KO cells were compared. Loss of Bcl6 significantly reduced the splenic and lymph node $CD4^+$ T cell populations as early as day 7 of infection, and this deficiency was amplified at memory time points. Bcl6 deficiency did not as severely impact $CD4^+$ T cell accumulation in the SI at day 7 compared to circulating subsets. However, by day 14 and 21 of infection, the frequency of Bcl6-KO cells was lower than that of WT cells (Fig. 7A,B). The differences in frequencies of WT and Bcl6-KO $CD4^+$ T cells were mirrored in the absolute cell counts (Fig. S7A,B). Consistent with the role of Bcl6 in T_{FH} differentiation, splenic Bcl6-KO $CD4^+$ T cells did not express CXCR5 and were predominantly $SLAM^+$ (Fig. S7C). The differential impact on $CD4^+$ T_{RM} between effector and memory time points was consistent with mRNA levels: day 7 IEL and LPL effector T cells expressed lower *Bcl6* than splenic samples, while day 21 SI IEL and LPL expressed *Bcl6* at higher levels than their circulating memory T cell counterparts (Fig. 2C). Furthermore, Bcl6-KO SI $CD4^+$ T cells displayed increased CD69 expression on day 7 and 21 and an early elevation of CD27 expression followed by a loss at day 21 compared to WT cells (Fig. S7D). Interestingly, while accumulation of $CD4^+$ T_{RM} required Bcl6, $CD8^+$ T_{RM} were unaffected by Bcl6 deletion at effector and memory time points, highlighting another difference in the T_{RM} transcriptional program between $CD4^+$ and $CD8^+$ T cells (Fig. S7E). We also examined the effect of Bcl6 deficiency in other mucosal barrier surfaces, including the liver, kidney, and lung, and saw that Bcl6-KO cells in tissues were similarly less impaired than their circulating counterparts compared to WT at day 7 (Fig. S7F).

To further assess the role of Bcl6 in early $CD4^+$ T_{RM} development, we performed bulk RNAseq of WT and Bcl6-KO SMARTA $CD4^+$ T cells at day 7 of infection. PCA analysis showed that loss of Bcl6 in splenic $CD4^+$ T cells led to a more T_H1-profile with splenic Bcl6-KO $CD4^+$ T cells grouping closely with T_H1 samples. SI Bcl6-KO $CD4^+$ T cells clustered closely with WT SI samples and were more similar to D21 IEL and LPL cells than their D7 WT counterparts (Fig. 7C). GSEA showed that D7 IEL and LPL Bcl6-KO cells were enriched for genes expressed by D21 SI cells and depleted for genes that were downregulated by D21 SI cells, suggesting that loss of Bcl6 accelerated progression of

effector T cells into mature T_{RM} (Fig. 7D). Additionally, loss of Bcl6 resulted in enrichment of the $CD4^+$ NLT gene signature by both splenic and SI populations and the $CD8^+$ T_{RM} gene signature by SI $CD4^+$ T cells, indicating that splenic Bcl6-KO cells upregulated genes indicative of T_{RM} more than WT cells. This conclusion is further supported by gene-expression signature analysis of scRNAseq data, with enrichment for the CD4 NLT and D20 SI genes in the Bcl6-KO SI populations at day 7 (Fig. 7E). Additionally, SI Bcl6-KO cells at day 7 expressed higher *Id2*, *Prdm1*, and *Cd69* than WT cells, suggesting that Bcl6 inhibits aspects of the T_{RM} program at early stages of the immune response (Fig. 7F). Interestingly, Runx3, a key regulator of $CD8^+$ T_{RM} (48) and known target of Bcl6 inhibition, also had higher expression in SI Bcl6-KO cells. However, shRNA knockdown of Runx3 in activated SMARTA $CD4^+$ T cells did not impair SI $CD4^+$ T cells compared to spleen (Fig. S7G). Collectively, our data demonstrate that Bcl6 is required to support the SI $CD4^+$ T_{RM} program, likely in maintaining the memory qualities of long-lived T_{RM} populations.

Discussion

In this study, we sought insights into the differentiation and transcriptional programming of the antiviral $CD4^+$ T_{RM} response. In the context of acute viral infection, we found that the early $CD4^+$ T_{RM} progenitor population in the SI was heterogenous and phenotypically, transcriptionally, and epigenetically similar to the recirculating splenic T_H1 population. At memory time points, $CD4^+$ T_{RM} expressed both T_H1/effector and T_{FH}/memory-associated genes, including co-expression of antagonistic factors, Blimp1 and Bcl6, in the same cells. We identified roles for Blimp1 and Id2 in supporting early $CD4^+$ T_{RM} development, while Bcl6 can mediate the maturation and/or persistence of $CD4^+$ T_{RM} with T_H1 characteristics in tissues. Multiple levels of regulation have been proposed for $CD4^+$ T_{RM} differentiation, including elements that dictate residency versus recirculation potential, determine $CD4^+$ versus $CD8^+$ lineage commitment, and regulate cellular responses to tissues-specific cues (11). Our study describes an additional level of regulation, one directing the effector versus memory identity of T_{RM} cells where $CD4^+$ T_{RM} acquire a gene-expression signature including TFs associated with both effector and memory cell fates, in order to balance the required rapid response of effector lymphocytes against the persistence and plasticity inherent in memory populations.

Our data highlight a shared phenotype and transcriptional profile for $CD4^+$ T_{RM} and T_H1 cells in response to acute infection. Circulating $CD4^+$ T cell populations were composed of both $SLAM^+$ T_H1 cells and $CXCR5^+$ T_{FH} cells, while tissue-resident $CD4^+$ T cells were predominantly $SLAM^+$ cells. This observation is consistent with studies in other infection models and tissues where $CD4^+$ T_{RM} cells reflected the T_H effector program associated with the acute pathogen/antigen exposure (16, 17, 19). At barrier surfaces, T_{RM} cells are among the first to encounter antigen and rapidly coordinate a local recall response (11, 12), which requires enhanced effector traits. Recent studies raised the possibility that $CD4^+$ T_{RM} could arise from, or in parallel to, T_{FH} cells. Given that fate-committed T_{FH} cells are the main proportion of the circulating $CD4^+$ memory T cell population (8), $CD4^+$ T_{RM} with T_{FH} characteristics (T_{FR}) in influenza infection have recently been reported (21, 22), and T_{FH} cells have a gene-expression pattern associated with memory cells and T cell survival.

However, our study shows that T_{RM} cells retained T_H1 effector functions and required both Blimp1 and Id2, critical factors in differentiation of effector T_H1 cells, consistent with circulating T_H1 effector cells serving as precursors of SI T_{RM}. Additionally, SI $CD4^+$ T_{RM} co-expressed effector- and memory-associated genes, suggesting that $CD4^+$ T_{RM} require some aspects of the memory/T_{FH} programs for their long-term maintenance and survival.

Given the established role of Blimp1 as a T_H1 fate-defining TF and a regulator of $CD8^+$ tissue residency (34, 37), it may be essential for both the T_H1 and tissue-residency aspects of the $CD4^+$ T_{RM} program. These observations are consistent with previous studies showing the function of Blimp1, and its family member Hobit, in regulating the transcriptional program of $CD8^+$ T_{RM} by inhibiting lymphocyte egress from the tissues, repressing the development of circulating memory cells (37), and driving $CD4^+$ T_{RM}-mediated colitis in human patients (54). We observed minimal Hobit expression and a clear requirement for Blimp1 in establishing SI $CD4^+$ T_{RM}. Blimp1-deficiency and Id2-deficiency separately led to a decrease in $CD4^+$ T cells in both the SI and spleen, especially within the T_H1 population. However, only loss of Blimp1 caused a significant reduction in SI cells compared to circulating splenic and mLN cells. This was consistent with Blimp1 regulating the expression of genes required for the migration into tissues or inhibiting genes that allow for egress (37), in addition to its role in T_H1 differentitiation. The role of Id2 in the T_{RM} program is likely due to its role in T_H1 differentiation, further supporting the hypothesis that T_{RM} and T_H1 cells are developmentally related.

We also examined the impact of deleting Bcl6, an essential T_{FH} and memory T cell-associated TF, on $CD4^+$ T_{RM} differentiation. During the effector phase, Bcl6-deficiency more dramatically impacted splenic $CD4^+$ T cells compared to the SI population. This is consistent with the known role of Bcl6 in repressing the T_H1 program in T_{FH} cells via inhibition of Blimp1 and Id2 (56), and in inhibiting the accumulation of lung T_H2 T_{RM} cells in an allergic house dust mite response (19). Furthermore, comparison of the transcriptional profiles of WT and Bcl6-KO cells at day 7 revealed an enrichment for T_{RM}-associated gene-expression signatures by Bcl6-KO $CD4^+$ T cells from the SI and within the splenic population. Surprisingly, by the memory time point, Bcl6 expression was upregulated in the T_{RM} population, with deletion of Bcl6 impairing the relative frequency and number of T_{RM} cells compared to the peak of the response. This may be because Bcl6 represses Klf2 in order for mature T_{RM} cells to maintain the low levels of S1pr1 and prevent recirculation, which we also observed in our bulk RNAseq analysis (27, 56). Bcl6-expressing T_{FH} cells share a transcriptional profile with $CD8^+$ memory-precursor T cells and contribute to the $CD4^+$ memory T cell population (8), suggesting that Bcl6 promotes long-lived $CD4^+$ and $CD8^+$ T cells. Thus, Bcl6 may actively enhance the memory attributes of the $CD4^+$ T_{RM} population.

Although $CD4^+$ T_{RM} populations were enriched for the core $CD8^+$ T_{RM} signature and similarly depended on Blimp1 and Bcl6 for early seeding of the SI, there were clear differences between the two T_{RM} lineages. SI $CD8^+$ T_{RM} cells expressed both CD69 and CD103 and accumulated in the SI epithelium and LP, while $CD4^+$ T_{RM} cells had minimal expression of CD103 and preferentially localized to the LP compartment. While effector $CD8^+$ T cells in tissues acquired much of the gene-expression profile of mature T_{RM}, $CD4^+$

T cells on day 7 of infection were distinct from the memory cells in the SI, requiring more time to fully upregulate the T_{RM} program. This observation is reminiscent of the stepwise transcriptional and genome accessibility changes described for $CD4^+$ CD8αα IEL (57), consistent with a time-dependent progression to tissue residency for $CD4^+$ T_{RM}. Previous work showed that $CD4^+$ T cells which migrate into the IEL upregulate Runx3 to become more cytotoxic $CD4^+CD8^+$αα cells (38); additionally, ectopic Runx3 expression can drive the TGF-β-transcriptional network in $CD4^+$ T_{RM}, promoting surivival, residency, and effector functions (36). However, we did not observe Runx3 dependence in the infection-driven response. This may be due to compensation by other Runx family proteins, such as Runx1 which is known to regulate $CD4^+$ T_{RM} formation (36), or other differences associated with $CD4^+CD8^+$αα cells. Interestingly, Bcl6 has been shown to inhibit Runx2 and Runx3 in day 7 T_{FH} cells (56). Thus, $CD4^+$ T_{RM} may fail to express sufficient Runx to drive the expression of CD103 and other key targets that mediate epithelial residence due to their concomitant upregulation of Bcl6. Additionally, accumulation of $CD4^+$ T_{RM} was accompanied by a requirement for Id2 but not Id3, whereas $CD8^+$ T_{RM} in the SI expressed both Id2 and Id3, with minimal defect arising from the Id2 deletion alone (55).

Here, we have highlighted the importance of Blimp1 and Id2 in establishing early effectors, and likely progenitors, of the $CD4^+$ T_{RM} SI population following viral infection. Blimp1 and Id2 presumably drive the T_H1-associated genes of the tissue-residency program, given the developmental relationship between T_H1 and T_{RM} cells. Surprisingly, Bcl6 also influenced T_{RM} formation, mediating repression of genes associated with mature T_{RM}, which may contribute to the erosion of $CD4^+$ T_{RM} populations. Further work is required to elucidate how $CD4^+$ T_{RM} are maintained in the tissues, particularly how Blimp1, Bcl6, and Id2 may interact in the T_{RM} gene-expression program at effector and memory stages. A better understanding of the transcriptional regulation of $CD4^+$ T_{RM} in the intestine will enhance our knowledge of T_{RM} directed immune responses in the context of long-term memory and how to target these cells for therapeutic purposes.

Material and Methods

Study design

The goal of this study was to determine the developmental origins and transcriptional regulation of $CD4^+$ T_{RM}. To test the developmental origins of $CD4^+$ $T_{RM,}$ TCR transgenic T cells were transferred into congenically distinct hosts, and the response to viral infection was observed and characterized by flow cytometry. Additionally, TCR transgenic T cells with various genotypes were also evaluated in response to viral infection to determine the transcriptional regulation of $CD4^+$ T_{RM}. The number of samples combined, number of replicates and statistical tests are listed in the figure legends.

Mice

All mice were housed under specific pathogen-free conditions in an American Association of Laboratory Animal Care–approved facility at the University of California, San Diego (UCSD), and all procedures were approved by the UCSD Institutional Animal Care and Use Committee. Blimp1-YFP mice (stock #008828;The Jackson Laboratory), Id3-GFP

mice(58), Id2-YFP mice(59), *Id2*$^{fl/fl}$ mice(60), CD4-Cre mice (stock#017336; The Jackson Laboratory), SMARTA mice (T cell receptor (TCR) transgenic for I-A^b-restricted LCMV glycoprotein amino acids $GP_{61–80}$ (61)), NIP mice (TCR transgenic for I-A^b restricted LCMV nucleoprotein (NP) peptide 311–325), P14 mice (TCR transgenic for H-2D^b-restricted LCMV glycoprotein $GP_{33–41}$; stock #037394-JAX; The Jackson Laboratory), CD45.1, and CD45.1.2 congenic mice were bred in house. *Bcl6*$^{f/f}$CD4-Cre$^+$CD45.1$^+$ SMARTA and *Prdm1*$^{f/f}$CD4-Cre$^+$CD45.1$^+$ SMARTA mice were received from the Crotty lab at the La Jolla Institute. Recipient C57BL/6J (B6) mice were either bred at UCSD or received from The Jackson Laboratory. Both male and female mice were used throughout the study, with sex and age matched T cell donors and recipients (or female donor cells transferred into male recipients). All animals used were between 6 weeks – 6 months of age.

T cell transfer and infection

Naive wild-type, Blimp1-YFP, Id2-YFP/Id3-GFP SMARTA CD4$^+$ T cells or wild-type P14 CD8$^+$ T cells congenically distinct for CD45 were adoptively transferred intravenously at $1×10^5$ SMARTA cells or $5×10^4$ P14 cells. For cotransfers, *Prdm1*$^{f/f}$CD4-Cre$^+$, *Id2*$^{f/f}$CD4-Cre$^+$, *Bcl6*$^{f/f}$CD4-Cre$^+$ and corresponding control SMARTA CD4$^+$ T cells or *Bcl6*$^{f/f}$CD4-Cre$^+$ and corresponding control P14 CD8$^+$ T cells were mixed in a 1:1 ratio and adoptively transferred at $1×10^5$ total cells per recipient mouse. Mice were then infected intraperitoneally with $2×10^5$ plaque-forming units (PFU) of lymphocytic choriomeningitis virus-Armstrong (LCMV-Arm) strain.

mLN sort-and-retransfer experiments

$1×10^5$ naive SMARTA CD4$^+$ T cells were adoptively transferred into recipients congenically distinct for CD45 and infected intraperitoneally with $2×10^5$ PFUs of LCMV-Arm. On day 6 of infection, mesenteric lymph nodes were removed, processed, and pooled. CD4$^+$ T Cells were enriched using MACS column depleting B cells, MHCII-expressing cells, and CD8$^+$ T cells. Enriched CD4$^+$ T cells were stained with antibodies for CD4, CD45.1, CD45.2, SLAM, and CXCR5 and T_H1 (SLAM$^+$) and T_{FH} (CXCR5$^+$) cells were sorted from sample. Sorted T_H1 and T_{FH} cells were then re-transferred into recipient mice which had been infected with LCMV-Arm for 3 days. On day 5 following re-transfer, cells were recovered from the spleen, mLN, and SI.

Antibodies, flow cytometry, and cell sorting

The following antibodies were used for surface staining (all from eBioscience unless otherwise specified): CD4 (GK1.5), CD45.1 (A20), CD45.2 (104), B220 (RA3–6B2, 1:400), SLAM (TC15–12F12.2, BioLegend), CD8 (53–6.7, BioLegend), CD69 (H1.2F3, Biolegend), CD103 (2E7), CD27 (LG.7F9), Ly6C (HK1.4, BioLegend), CD199/CCR9 (eBioCW-1.2), CD49d (R1–2), P2Rx7 (1F11, BioLegend), FR4 (12A5, BioLegend), NKG2A/C/E (20d5, Invitrogen), NK1.1 (PK136, eBioscience), PSGL-1 (4RA10, Invitrogen),), CD90.2 (30-H12, Biolegend). Cells were incubated for 30 minutes at 4°C in PBS supplemented with 2% bovine growth serum and 0.1% sodium azide, unless specified otherwise. CXCR5 staining was performed by incubating cells with purified anti-CXCR5 (SPRCL5, 1:50; Invitrogen), followed by PE-Cy7- or BV510-labeled streptavidin (1:1000, eBioscience) each for 30 minutes at 4°C. Intracellular staining was performed

using the eBioscience FOXP3/Transcription Factor Staining Buffer Set and the following antibodies: Granzyme A (3G8.5, BioLegend), Granzyme B (GB12, LifeTech), IFNγ (XMG1.2, BioLegend), IL-2 (JES6–5H4), and TNFα (MP6-XT22). For cytokine staining, $CD4^+$ T cells from the spleens, lymph nodes, and SI were incubated for 6 hours at 37°C in RPMI-1640 media containing 10% (v/v) bovine growth serum with 10nM $GP_{66–81}$ peptide and Protein Transport Inhibitor (eBioscience). Stained cells were analyzed using LSRFortessa or LSRFortessa X-20 cytometers (BD) and FlowJo software (TreeStar). All sorting was performed on the BD FACSAria instrument.

Sequencing

Methods for bulk RNA seq, scRNAseq and ATACseq can be found in Supplementary Matrials.

Statistical methods

Statistical tests were performed using Prism (7.0/9.0) (Graphpad). Two-tailed paired t-test was used for comparisons between 2 groups, while one-way ANOVA test was used for comparisons between 2+ groups. P values of <0.05 were considered significant.

Supplementary Material

Refer to Web version on PubMed Central for supplementary material.

Acknowledgments

We would like to thank the members of the Goldrath, Chang, and Crotty laboratories for technical advice and thoughtful discussion, in particular, Anh Nguyen for experimental assistance, Kyla Omilusik for critical reading of the manuscript, Nathaniel Bloom for Blimp1-KO and Bcl6-KO mice, and Lauren Quezada for help with single-cell RNAseq library preparation. Single-cell RNA sequencing using the 10X Genomics platform was conducted at the IGM Genomics Center, University of California, San Diego, La Jolla, CA.

Funding

Funding provided by the National Institutes of Health (R01AI067545 to AWG, U19AI109976 and P01AI145815 to A.W.G, S.C, and M.P), the American Heart Association (18PRE33960263 to Q.P.N.), the German Research Foundation Fellowship (HE 8656/1–1 to M.H), and the Ruth L. Kirschstein National Research Service Award (NRSA) Institutional Research Training Grants (T32) (AR064194 to T.D.). We thank the Immunological Genome Project (ImmGen) for reagents and sample/data processing. A.W.G. is the Tata Chancellor's Professor (V) in the Division of Biological Sciences. IGM Genomics Center is supported by grants P30KC063491 and P30CA023100.

Data and materials availaiblity

RNA-seq and ATAC–seq data were deposited to the Gene Expression Omnibus (GEO) under the GSE184263 super series. All data needed to evaluate the conclusions in the paper are present in the paper or the Supplementary Materials.

References

1. Zhu J, Yamane H, Paul WE, Differentiation of Effector CD4 T Cell Populations. Annu. Rev. Immunol 28, 445–89 (2010). [PubMed: 20192806]
2. Williams MA, V Ravkov E, Bevan MJ, Rapid Culling of the CD4 + T Cell Repertoire in the Transition from Effector to Memory. Immunity. 28, 533–545 (2008). [PubMed: 18356084]

3. Pepper M, Linehan JL, Pagán AJ, Zell T, Dileepan T, Cleary PP, Jenkins MK, Different routes of bacterial infection induce long-lived TH1 memory cells and short-lived TH17 cells. Nat. Immunol 11, 83–89 (2010). [PubMed: 19935657]
4. Pepper M, Pagán AJ, Igyá BZ, Taylor JJ, Jenkins MK, Igyártó BZ, Taylor JJ, Jenkins MK, Opposing Signals from the Bcl6 Transcription Factor and the Interleukin-2 Receptor Generate T Helper 1 Central and Effector Memory Cells. Immunity. 35, 583–595 (2011). [PubMed: 22018468]
5. Hale JS, Youngblood B, Latner DR, Ur A, Mohammed R, Ye L, Akondy RS, Wu T, Iyer SS, Ahmed R, Mohammed AUR, Ye L, Akondy RS, Wu T, Iyer SS, Ahmed R, Distinct memory CD4+ T cells with commitment to T follicular helper- and T helper 1-cell lineages are generated after acute viral infection. Immunity. 38, 805–817 (2013). [PubMed: 23583644]
6. Künzli M, Schreiner D, Pereboom TC, Swarnalekha N, Litzler LC, Lötscher J, Ertuna YI, Roux J, Geier F, Jakob RP, Maier T, Hess C, Taylor JJ, King CG, Long-lived T follicular helper cells retain plasticity and help sustain humoral immunity. Sci. Immunology 5, (2020).
7. Ciucci T, Vacchio MS, Gao Y, Ardori FT, Candia J, Mehta M, Zhao Y, Tran B, Pepper M, Tessarollo L, McGavern DB, Bosselut R, The Emergence and Functional Fitness of Memory CD4+ T Cells Require the Transcription Factor Thpok. Immunity. 50, 91–105 (2019). [PubMed: 30638736]
8. Choi YS, Yang JA, Yusuf I, Johnston RJ, Greenbaum J, Peters B, Crotty S, Bcl6 Expressing Follicular Helper CD4 T cells are Fate Committed Early and Have the Capacity to Form Memory. J. Immunol 190, 4014–4026 (2013). [PubMed: 23487426]
9. Nguyen QP, Deng TZ, Witherden DA, Goldrath AW, Origins of CD4 + circulating and tissue-resident memory T-cells. Immunology. 157, 3–12 (2019). [PubMed: 30897205]
10. Mueller SN, Mackay LK, Tissue-resident memory T cells: Local specialists in immune defence. Nat. Rev. Immunol 16, 78–89 (2016).
11. Beura LK, Fares-Frederickson NJ, Steinert EM, Scott MC, Thompson EA, Fraser KA, Schenkel JM, Vezys V, Masopust D, CD4 + resident memory T cells dominate immunosurveillance and orchestrate local recall responses. J. Exp. Med 216, 1214–1229 (2019). [PubMed: 30923043]
12. Pruner KB, Pepper M, Local memory CD4 T cell niches in respiratory viral infection. J. Exp. Med 218 (2021).
13. Collins N, Jiang X, Zaid A, Macleod BL, Li J, Park CO, Haque A, Bedoui S, Heath WR, Mueller SN, Kupper TS, Gebhardt T, Carbone FR, Skin CD4+ memory T cells exhibit combined cluster-mediated retention and equilibration with the circulation. Nat. Commun 7 (2016).
14. Glennie ND, Yeramilli VA, Beiting DP, Volk SW, Weaver CT, Scott P, Skin-resident memory CD4+ T cells enhance protection against Leishmania major infection. J. Exp. Med 212, 1405–1414 (2015). [PubMed: 26216123]
15. Iijima N, Iwasaki A, A local macrophage chemokine network sustains protective tissue-resident memory CD4 T cells. Science. 346, 93–98 (2014). [PubMed: 25170048]
16. Hondowicz BD, Kim KS, Ruterbusch MJ, Keitany GJ, Pepper M, IL-2 is required for the generation of viral-specific CD4+Th1 tissue-resident memory cells and B cells are essential for maintenance in the lung. Eur. J. Immunol 48, 80–86 (2018). [PubMed: 28948612]
17. Amezcua Vesely MC, Pallis P, Bielecki P, Low JS, Zhao J, Harman CCD, Kroehling L, Jackson R, Bailis W, Licona-Limón P, Xu H, Iijima N, Pillai PS, Kaplan DH, Weaver CT, Kluger Y, Kowalczyk MS, Iwasaki A, Pereira JP, Esplugues E, Gagliani N, Flavell RA, Effector TH17 Cells Give Rise to Long-Lived TRM Cells that Are Essential for an Immediate Response against Bacterial Infection. Cell. 178, 1176–1188.e15 (2019). [PubMed: 31442406]
18. Romagnoli P, Fu H, Qiu Z, Khairallah C, Pham Q, Puddington L, Khanna K, Lefrançois L, Sheridan B, Differentiation of distinct long-lived memory CD4 T cells in intestinal tissues after oral Listeria monocytogenes infection. Mucosal Immunol. 10, 520–530 (2017). [PubMed: 27461178]
19. Hondowicz BD, An D, Schenkel JM, Altemeier WA, Masopust D, Kim KS, Steach HR, Krishnamurty AT, Keitany GJ, Garza EN, Fraser KA, Moon JJ, Pepper M, Interleukin-2-Dependent Allergen-Specific Tissue-Resident Memory Cells Drive Asthma. Immunity. 44, 155–166 (2016). [PubMed: 26750312]

20. Johnston RJ, Poholek AC, DiToro D, Yusuf I, Eto D, Barnett B, Dent AL, Craft J, Crotty S, Bcl6 and Blimp-1 Are Reciprocal and Antagonistic Regulators of T Follicular Helper Cell Differentiation. Science. 325 (2009).
21. Swarnalekha N, Schreiner D, Litzler LC, Iftikhar S, Kirchmeier D, Künzli M, Son YM, Sun J, Moreira EA, King CG, T resident helper cells promote humoral responses in the lung. Sci. Immunology 6, (2021).
22. Son YM, Cheon IS, Wu Y, Li C, Wang Z, Gao X, Chen Y, Takahashi Y, Fu Y-X, Dent AL, Kaplan MH, Taylor JJ, Cui W, Sun J, Tissue-resident CD4 + T helper cells assist the development of protective respiratory B and CD8 + T cell memory responses. Sci. Immunology 6, (2021).
23. Botta D, Fuller MJ, Marquez-Lago TT, Bachus H, Bradley JE, Weinmann AS, Zajac AJ, Randall TD, Lund1 FE, León B, Ballesteros-Tato A, Dynamic regulation of T follicular regulatory cell responses by interleukin 2 during influenza infection. Nat. Immunol 18 (2017).
24. Wing JB, Kitagawa Y, Locci M, Hume H, Tay C, Morita T, Kidani Y, Matsuda K, Inoue T, Kurosaki T, Crotty S, Coban C, Ohkura N, Sakaguchi S, Graca L, Hori S, A distinct subpopulation of CD25 T-follicular regulatory cells localizes in the germinal centers. PNAS. (2017).
25. Peng C, Jameson SC, The relationship between CD4+ follicular helper T cells and CD8+ resident memory T cells: Sisters or distant cousins? Int. Immunol 32 (2020), pp. 583–587. [PubMed: 32620009]
26. Walsh DA, Borges da Silva H, Beura LK, Peng C, Hamilton SE, Masopust D, Jameson SC, The Functional Requirement for CD69 in Establishment of Resident Memory CD8 + T Cells Varies with Tissue Location. J. Immunol 203, 946–955 (2019). [PubMed: 31243092]
27. Skon CN, Lee JY, Anderson KG, Masopust D, Hogquist KA, Jameson SC, Transcriptional downregulation of S1pr1 is required for the establishment of resident memory CD8+ T cells. Nat. Immunol 14, 1285–1293 (2013). [PubMed: 24162775]
28. Lee JY, Skon CN, Lee YJ, Oh S, Taylor JJ, Malhotra D, Jenkins MK, Rosenfeld MG, Hogquist KA, Jameson SC, The Transcription Factor KLF2 Restrains CD4+ T Follicular Helper Cell Differentiation. Immunity. 42, 252–264 (2015). [PubMed: 25692701]
29. Weber JP, Fuhrmann F, Feist RK, Lahmann A, Al Baz MS, Gentz LJ, Vu Van D, Mages HW, Haftmann C, Riedel R, Grün JR, Schuh W, Kroczek RA, Radbruch A, Mashreghi MF, Hutloff A, ICOS maintains the T follicular helper cell phenotype by down-regulating krüppel-like factor 2. J. Exp. Med 212, 217–233 (2015). [PubMed: 25646266]
30. He J, Tsai LM, Leong YA, Hu X, Ma CS, Chevalier N, Sun X, Vandenberg K, Rockman S, Ding Y, Zhu L, Wei W, Wang C, Karnowski A, Belz GT, Ghali JR, Cook MC, Riminton DS, Veillette A, Schwartzberg PL, Mackay F, Brink R, Tangye SG, Vinuesa CG, Mackay CR, Li Z, Yu D, Circulating Precursor CCR7 lo PD-1 hi CXCR5 + CD4 + T Cells Indicate Tfh Cell Activity and Promote Antibody Responses upon Antigen Reexposure. Immunity. 39, 770–781 (2013). [PubMed: 24138884]
31. Kumar BV, Ma W, Miron M, Granot T, Guyer RS, Carpenter DJ, Senda T, Sun X, Ho SH, Lerner H, Friedman AL, Shen Y, Farber DL, Human Tissue-Resident Memory T Cells Are Defined by Core Transcriptional and Functional Signatures in Lymphoid and Mucosal Sites. Cell Rep. 20, 2921–2934 (2017). [PubMed: 28930685]
32. Crotty S, Johnston RJ, Schoenberger SP, Effectors and memories: Bcl-6 and Blimp-1 in T and B lymphocyte differentiation. Nat. Immunol 11, 114–120 (2010). [PubMed: 20084069]
33. Fu S-H, Yeh L-T, Chu C-C, Lin-Ju Yen B, Sytwu H-K, New insights into Blimp-1 in T lymphocytes: a divergent regulator of cell destiny and effector function. J. Biomed. Sci 24 (2017).
34. Cimmino L, Martins GA, Liao J, Magnusdottir E, Grunig G, Perez RK, Calame KL, Blimp-1 Attenuates Th1 Differentiation by Repression of ifng, tbx21, and bcl6 Gene Expression. J. Immunol 181, 2338–2347 (2008). [PubMed: 18684923]
35. Kohu K, Ohmori H, Wong WF, Onda D, Wakoh T, Kon S, Yamashita M, Nakayama T, Kubo M, Satake M, The Runx3 Transcription Factor Augments Th1 and Down-Modulates Th2 Phenotypes by Interacting with and Attenuating GATA3. J. Immunol 183, 7817–7824 (2009). [PubMed: 19933870]
36. Fonseca R, Burn TN, Gandolfo LC, Devi S, Park SL, Obers A, Evrard M, Christo SN, Buquicchio FA, Lareau CA, McDonald KM, Sandford SK, Zamudio NM, Zanluqui NG, Zaid A, Speed

TP, Satpathy AT, Mueller SN, Carbone FR, Mackay LK, Runx3 drives a CD8+ T cell tissue residency program that is absent in CD4+ T cells. Nat. Immunol 23, 1236–1245 (2022). [PubMed: 35882933]

37. Mackay LK, Minnich M, Kragten NAM, Liao Y, Nota B, Seillet C, Zaid A, Man K, Preston S, Freeston D, Braun A, Wynne-Jones E, Behr FM, Stark R, Pellicci DG, Godfrey DI, Belz GT, Pellegrini M, Gebhardt T, Busslinger M, Shi W, Carbone FR, van Lier RAW, Kallies A, van Gisbergen KPJM, Hobit and Blimp1 instruct a universal transcriptional program of tissue residency. Science. 352, 459–463 (2016). [PubMed: 27102484]
38. Reis BS, Rogoz A, Costa-Pinto FA, Taniuchi I, Mucida D, Mutual expression of the transcription factors Runx3 and ThPOK regulates intestinal CD4+ T cell immunity. Nat. Immunol 14, 271–280 (2013). [PubMed: 23334789]
39. Shaw LA, Belanger S, Omilusik KD, Cho S, Scott-Browne JP, Nance JP, Goulding J, Lasorella A, Lu L-F, Crotty S, Goldrath AW, Id2 reinforces TH1 differentiation and inhibits E2A to repress TFH differentiation. Nat. Immunol 17, 834–843 (2016). [PubMed: 27213691]
40. Omilusik K, Shaw L, Goldrath A, Remembering one's ID/E-ntity: E/ID protein regulation of T cell memory. Curr. Opin. Immunol 25, 660–6 (2013). [PubMed: 24094885]
41. Shaw LA, Deng TZ, Omilusik KD, Takehara KK, Nguyen QP, Goldrath AW, Id3 expression identi fi es CD4 + memory Th1 cells. PNAS. 119 (2022).
42. Masopust D, Vezys V, John Wherry E, Barber DL, Ahmed R, Cutting Edge: Gut Microenvironment Promotes Differentiation of a Unique Memory CD8 T Cell Population. J Immunol. 176, 2079–2083 (2006). [PubMed: 16455963]
43. Hendriks J, Gravestein LA, Tesselaar K, Van Lier RAW, Schumacher TNM, Borst J, CD27 is required for generation and long-term maintenance of T cell immunity. Nat. Immunol 1, 433–440 (2000). [PubMed: 11062504]
44. Fritsch RD, Shen X, Sims GP, Hathcock KS, Hodes RJ, Lipsky PE, Stepwise Differentiation of CD4 Memory T Cells Defined by Expression of CCR7 and CD27. J. Immunol 175, 6489–6497 (2005). [PubMed: 16272303]
45. Schiött Å, Lindstedt M, Johansson-Lindbom B, Roggen E, Borrebaeck CAK, CD27- CD4+ memory T cells define a differentiated memory population at both the functional and transcriptional levels. Immunology. 113, 363–370 (2004). [PubMed: 15500623]
46. Marshall HD, Chandele A, Jung YW, Meng H, Poholek AC, Parish IA, Rutishauser R, Cui W, Kleinstein SH, Craft J, Kaech SM, Differential Expression of Ly6C and T-bet Distinguish Effector and Memory Th1 CD4+ Cell Properties during Viral Infection. Immunity. 35, 633–646 (2011). [PubMed: 22018471]
47. Nance JP, Bélanger S, Johnston RJ, Takemori T, Crotty S, Cutting Edge: T Follicular Helper Cell Differentiation Is Defective in the Absence of Bcl6 BTB Repressor Domain Function. DCSupplemental J. Immunol. by guest April 194, 5599–5603 (2015).
48. Milner JJ, Toma C, Yu B, Zhang K, Omilusik K, Phan AT, Wang D, Getzler AJ, Nguyen T, Crotty S, Wang W, Pipkin ME, Goldrath AW, Runx3 programs CD8+ T cell residency in non-lymphoid tissues and tumours. Nat. Publ. Gr 552 (2017).
49. Masopust D, Choo D, Wherry J, Newell K, Ahmed R, Dynamic T cell migration program provides resident memory within intestinal epithelium. J. Exp. Med 207, 553–564 (2010). [PubMed: 20156972]
50. Marshall NB, Swain SL, Cytotoxic CD4 T cells in antiviral immunity. J. Biomed. Biotechnol 2011 (2011).
51. Marshall NB, Vong AM, Devarajan P, Brauner MD, Kuang Y, Nayar R, Schutten EA, Castonguay CH, Berg LJ, Nutt SL, Swain SL, NKG2C/E Marks the Unique Cytotoxic CD4 T Cell Subset, ThCTL, Generated by Influenza Infection. J. Immunol 198, 1142–1155 (2017). [PubMed: 28031335]
52. Chang JT, Wherry EJ, Goldrath AW, Molecular regulation of effector and memory T cell differentiation. Nat. Immunol. Rev 15, 1104–1115 (2014).
53. Yu B, Zhang K, Milner JJ, Toma C, Chen R, Scott-Browne JP, Pereira RM, Crotty S, Chang JT, Pipkin ME, Wang W, Goldrath AW, Epigenetic landscapes reveal transcription factors that regulate CD8+ T cell differentiation. Nat. Immunol 18, 573–582 (2017). [PubMed: 28288100]

54. Zundler S, Becker E, Spocinska M, Slawik M, Parga-Vidal L, Stark R, Wiendl M, Atreya R, Rath T, Leppkes M, Hildner K, López-Posadas R, Lukassen S, Ekici AB, Neufert C, Atreya I, van Gisbergen KPJM, Neurath MF, Hobit- and Blimp-1-driven CD4 + tissue-resident memory T cells control chronic intestinal inflammation. Nat. Immunol 20, 288–300 (2019). [PubMed: 30692620]

55. Milner JJ, Toma C, He Z, Kurd NS, Nguyen QP, McDonald B, Quezada L, Widjaja CE, Witherden DA, Crowl JT, Shaw LA, Yeo GW, Chang JT, Omilusik KD, Goldrath AW, Heterogenous Populations of Tissue-Resident CD8+ T Cells Are Generated in Response to Infection and Malignancy. Immunity. 52, 808–824.e7 (2020). [PubMed: 32433949]

56. Choi J, Diao H, Faliti CE, Truong J, Rossi M, Bélanger S, Yu B, Goldrath AW, Pipkin ME, Crotty S, Bcl-6 is the nexus transcription factor of T follicular helper cells via repressor-of-repressor circuits. Nat. Immunol 21, 777–789 (2020). [PubMed: 32572238]

57. London M, Bilate AM, Castro TBR, Sujino T, Mucida D, Stepwise chromatin and transcriptional acquisition of an intraepithelial lymphocyte program. Nat. Immunol. 2021 224 22, 449–459 (2021).

58. Miyazaki M, Rivera RR, Miyazaki K, Lin YC, Agata Y, Murre C, The opposing roles of the transcription factor E2A and its antagonist Id3 that orchestrate and enforce the naive fate of T cells. Nat. Immunol 12, 992–1001 (2011). [PubMed: 21857655]

59. Yang CY, Best JA, Knell J, Yang E, Sheridan AD, Jesionek AK, Li HS, Rivera RR, Lind KC, D'Cruz LM, Watowich SS, Murre C, Goldrath AW, The transcriptional regulators Id2 and Id3 control the formation of distinct memory CD8 + T cell subsets. Nat. Immunol 12, 1221–1229 (2011). [PubMed: 22057289]

60. Niola F, Zhao X, Singh D, Castano A, Sullivan R, Lauria M, Nam HS, Zhuang Y, Benezra R, Di Bernardo D, Iavarone A, Lasorella A, Id proteins synchronize stemness and anchorage to the niche of neural stem cells. Nat. Cell Biol 14, 477–487 (2012). [PubMed: 22522171]

61. Oxenius A, Bachmann MF, Zinkernagel RM, Hengartner H, Virus-specific MHC class II-restricted TCR-transgenic mice: effects on humoral and cellular immune responses after viral infection. Eur. J. Immunol 28, 390–400 (1998). [PubMed: 9485218]

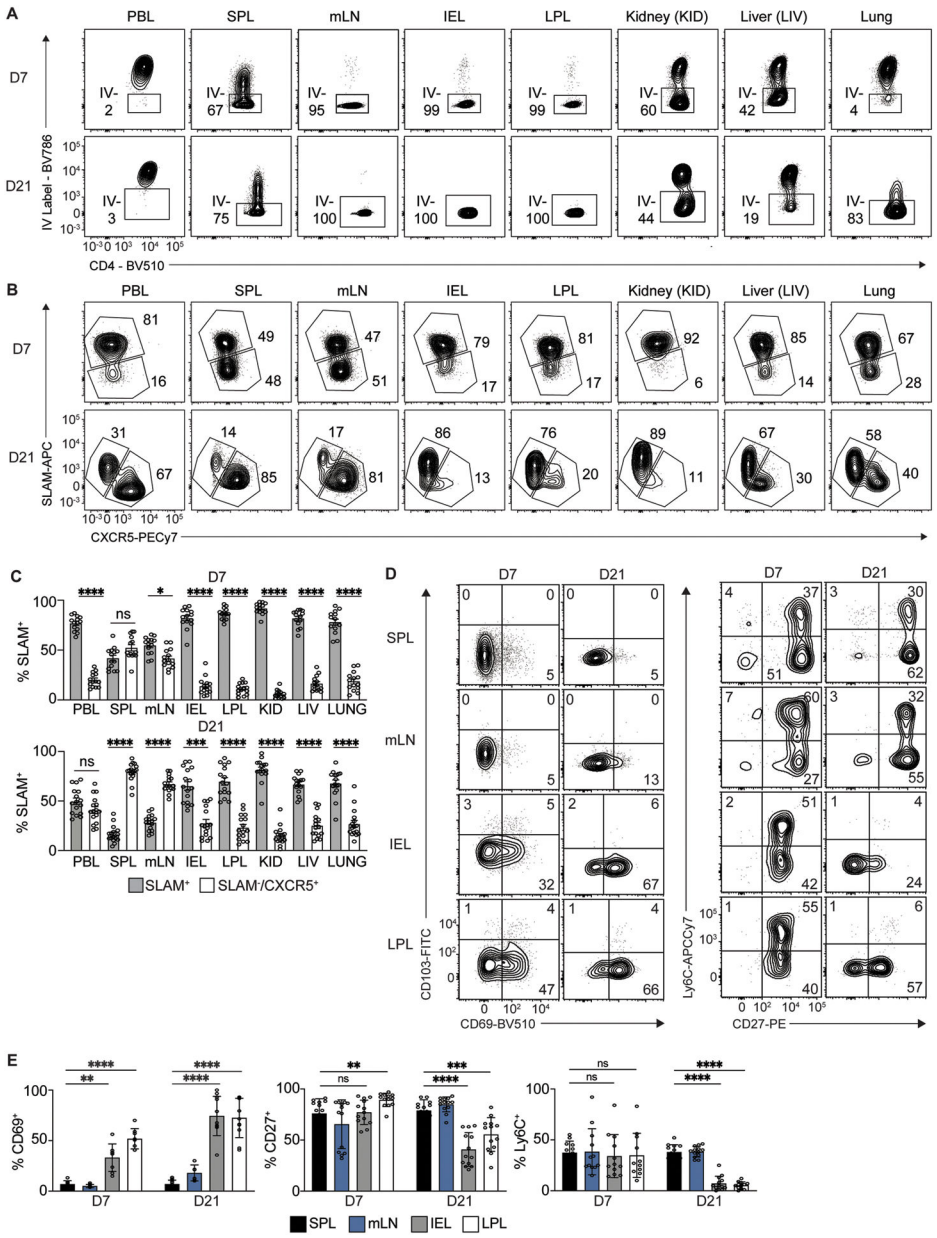

Figure 1. CD4$^+$ T$_{RM}$ retain a T$_H$1 effector cell profile during viral infection.

Naive SMARTA CD4$^+$ T cells were transferred into congenically distinct mice that were subsequently infected with LCMV-Arm. On days 7 and 21 of infection, SMARTA CD4$^+$ T cells were isolated**. (A)** Representative flow plots showing frequency of IV$^-$ SMARTA cells in peripheral blood (PBL), spleen (SPL), mesenteric lymph nodes (mLN), intraepithelial lymphocytes (IEL) and lamina propria lymphocytes (LPL) from the small intestine (SI), kidney (KID), liver (LIV), and lung on indicated day of infection. **(B-C)** Expression of SLAM and CXCR5 by SMARTA CD4$^+$ T cells in PBL, SPL, mLN, IEL, LPL, kidney, liver, and lung on indicated day of infection. Representative flow cytometry plots (B) and quantification (C) of SLAM$^+$ and SLAM$^-$CXCR5$^+$ SMARTA CD4$^+$ T cells. (**D-E**) Expression of CD69, CD103, CD27 and Ly6C by SMARTA CD4$^+$ T cells in SPL, mLN,

IEL, and LPL on indicated day of infection. Representative flow cytometry plots (D) and quantification (E) of frequencies of $CD69^+$, $CD27^+$, and $Ly6C^+$ cells. Numbers in flow plots indicate percent of cells in corresponding gate. Data are representative (A,B) or cumulative (C,E) of 3 experiments (A-E) with n=2–4 mice. Graphs show mean ± SD; *p < 0.05, ** p<0.01, *** p<0.001, ****p< 0.0001. Paired t-test (C) or one-way ANOVA test (E) was performed for statistical significance.

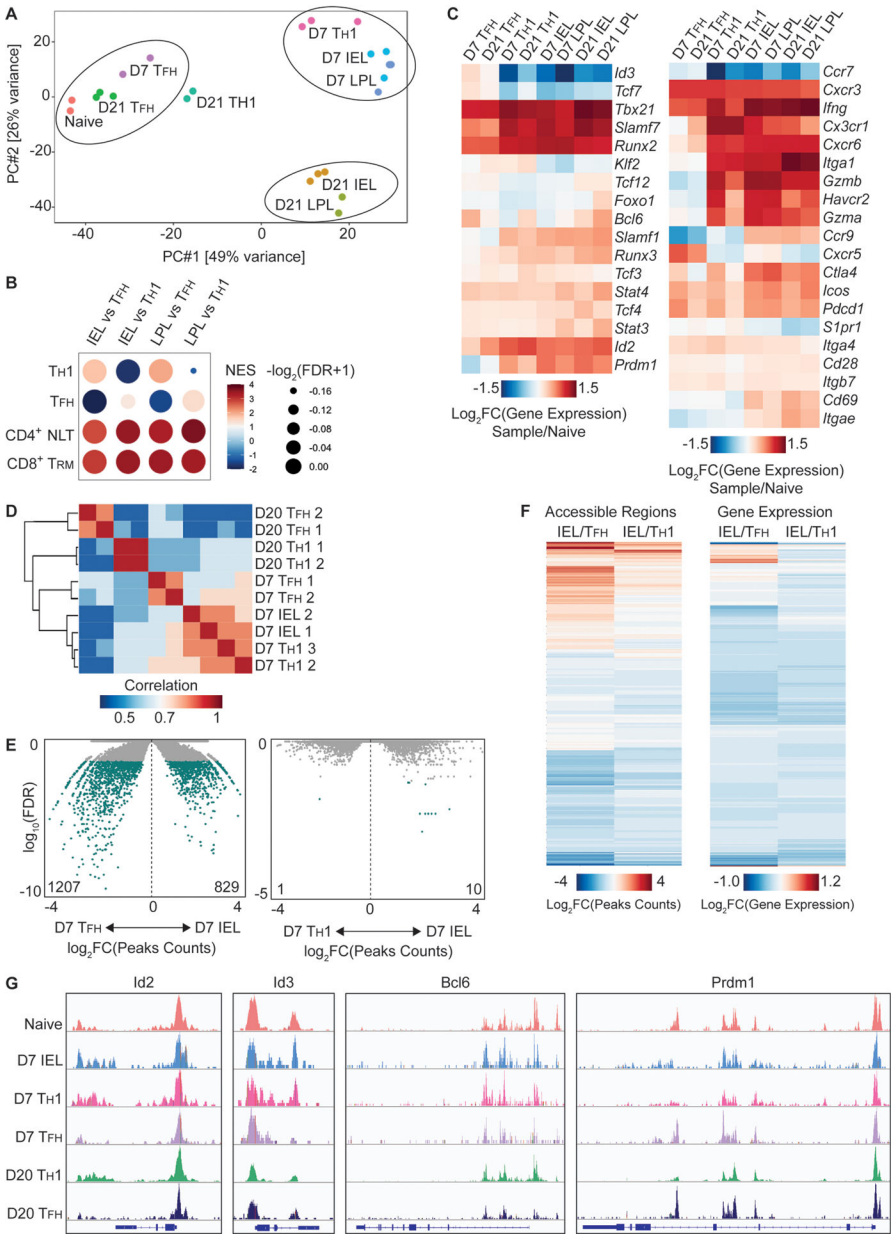

Figure 2. CD4$^+$ T_{RM} in viral infections are transcriptionally and epigenetically similar to T_H1 cells.

(A) Principal component analysis (PCA) of bulk RNAseq of circulating and resident SMARTA CD4$^+$ T cells from spleen and SI, harvested on day 7 or 21 of LCMV-Arm infection. **(B)** Gene set enrichment analysis (GSEA) of day 21 RNAseq data. **(C)** Heatmap showing gene expression of transcriptional regulators (left) or cell surface receptors/ cytokines (right). Values are calculated as a log_2fold change between each sample and naive population. **(D-G)** ATACseq of circulating and resident SMARTA CD4$^+$ T cells from spleen and IEL on day 7 or spleen on day 20 of infection. **(D)** Pearson correlation for peaks in differentially accessible regions. **(E)** Volcano plots comparing peak counts between D7 IEL and T_H1 or T_{FH} subsets. Numbers in volcano plots indicate number of differentially accessible regions in IEL compared to either T_H1 or T_{FH} samples. **(F)** Left, heatmap

showing differentially accessible regions (DARs) between IEL compared to splenic T_{FH} or T_H1 populations. Right, heatmap showing expression of genes corresponding to DARs. Values are calculated as a $\log_2$fold change between IEL and T_{FH} or T_H1. **(G)** Genome browser tracks depict ATACseq chromatin accessibility across samples for indicated gene. Data from average of 3 replicates (A-C) or 2 replicates (D-G) with cells pooled from 4–5 mice per replicate for day 7 and n=12–15 mice per replicate for day 21.

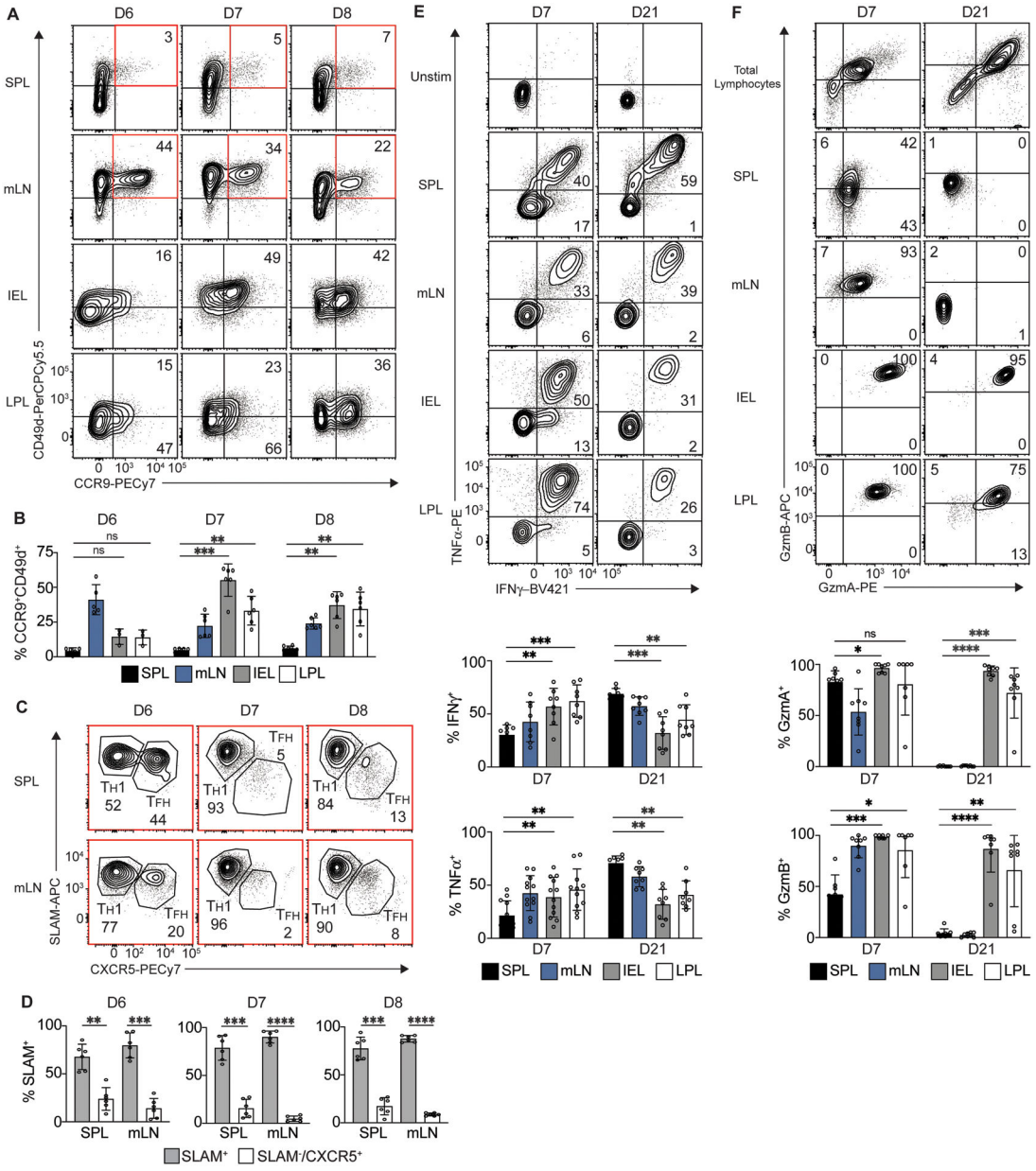

Figure 3. T_H1 effector cells from the spleen and mLNs express gut homing molecules.

(A-B) CCR9 and CD49d expression by $CD4^+$ T cells in specified tissues on days 6–8 of LCMV-Arm infection. Representative flow cytometry plots (A), and quantification (B) of $CCR9^+CC49d^+$ SMARTA $CD4^+$ T cells. $CCR9^+CD49d^+$ quadrants are highlighted in red **(C-D)** Expression of SLAM and CXCR5 by $CCR9^+CC49d^+$ SMARTA $CD4^+$ T cells in the spleen or mLN on days 6–8 of LCMV-Arm infection. Representative flow cytometry plots (C) and quantification (D) of T_H1 ($SLAM^+CXCR5^-$) and T_{FH} ($SLAM^-CXCR5^+$) SMARTA cells. **(E)** IFNγ and TNFα expression by $CD4^+$ T cells on indicated day of infection following *ex vivo* $GP_{61–80}$ peptide stimulation in specified tissues. Representative flow cytometry plots (top) and quantification (bottom) of $IFN\gamma^+$ and $TNF\alpha^+$ SMARTA $CD4^+$ T cells. **(F)** Granzyme A (GzmA) and B (GzmB) expression by SMARTA $CD4^+$ T cells in

specified tissues on indicated day of infection. Representative flow cytometry plots (top) and quantification (bottom) of $GzmA^+$ and $GzmB^+$ SMARTA $CD4^+$ T cells. Numbers in flow plots indicate frequency of cells in corresponding gate. Data are representative (A,C,E,F) or cumulative (B,D,E,F) of 2 experiments with n=3–4 mice. Graphs show mean ± SD; *p < 0.05, ** p<0.01, *** p<0.001, ****p< 0.0001. One-way ANOVA (B, E-F) or paired t-test (D) were performed for statistical significance.

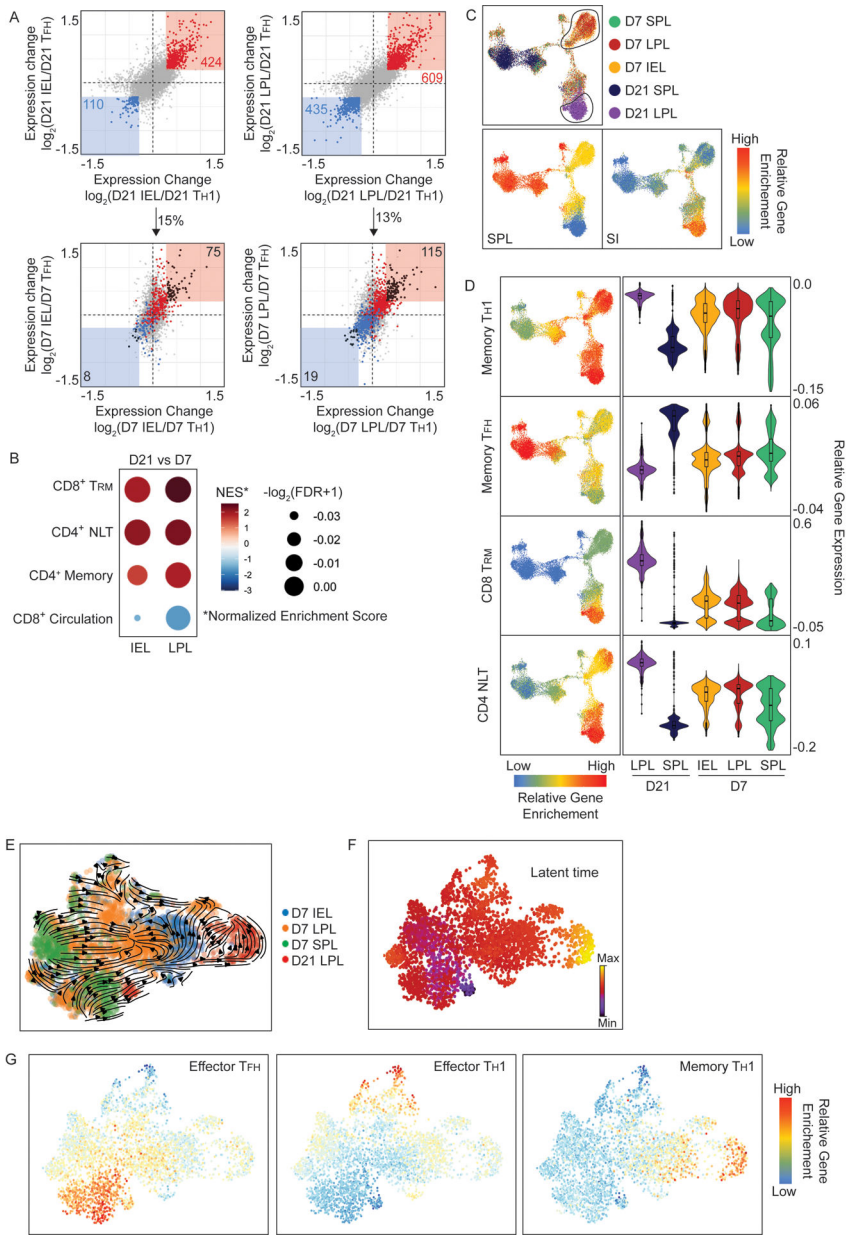

Figure 4. Effector SI CD4$^+$ T cells in viral infection progress towards a mature T_{RM} program.

(A) Top, comparison of gene expression of IEL (left) and LPL (right) CD4$^+$ T_{RM} cells relative to T_H1 and T_{FH} subsets on day 21 of LCMV infection. Red denotes genes with increased expression in T_{RM} relative to T_H1 and T_{FH} cells; blue denotes genes with increased expression in T_H1 and T_{FH} relative to T_{RM} cells. Bottom, comparison of differentially expressed genes in mature T_{RM} cells (from top panel) in cells from IEL or LPL on day 7 of infection. Black denotes genes from top panel (either blue or red) which are differentially expressed by day 7 SI SMARTA CD4$^+$ T cells compared to day 7 splenic SMARTA CD4$^+$ T cell subsets. **(B)** Gene set enrichment analysis (GSEA) comparing day 7 and 21 SI SMARTA CD4$^+$ T cells. **(C-G)** Single-cell RNAseq of circulating and resident SMARTA CD4$^+$ T cells from spleen and SI, harvested on day 7 or 21 post-infection. **(C)**

UMAP dimensional reduction colored by sample (top) and relative enrichment of indicated gene signatures (bottom). **(D)** UMAP reduction and violin plots showing relative enrichment of indicated gene signatures. **(E)** Velocity field projected onto UMAP plot of specified tissues. Arrows show the local average velocity evaluated on a regular grid. (**F)** UMAP plots showing latent time with yellow representing the most terminal state. (**G)** UMAP plots showing enrichment of specified gene signature. Data are from 2–3 replicates (A-C) or 2 replicates (D-H) of cells pooled from 4–5 mice for day 7 and n=12–15 mice for day 21.

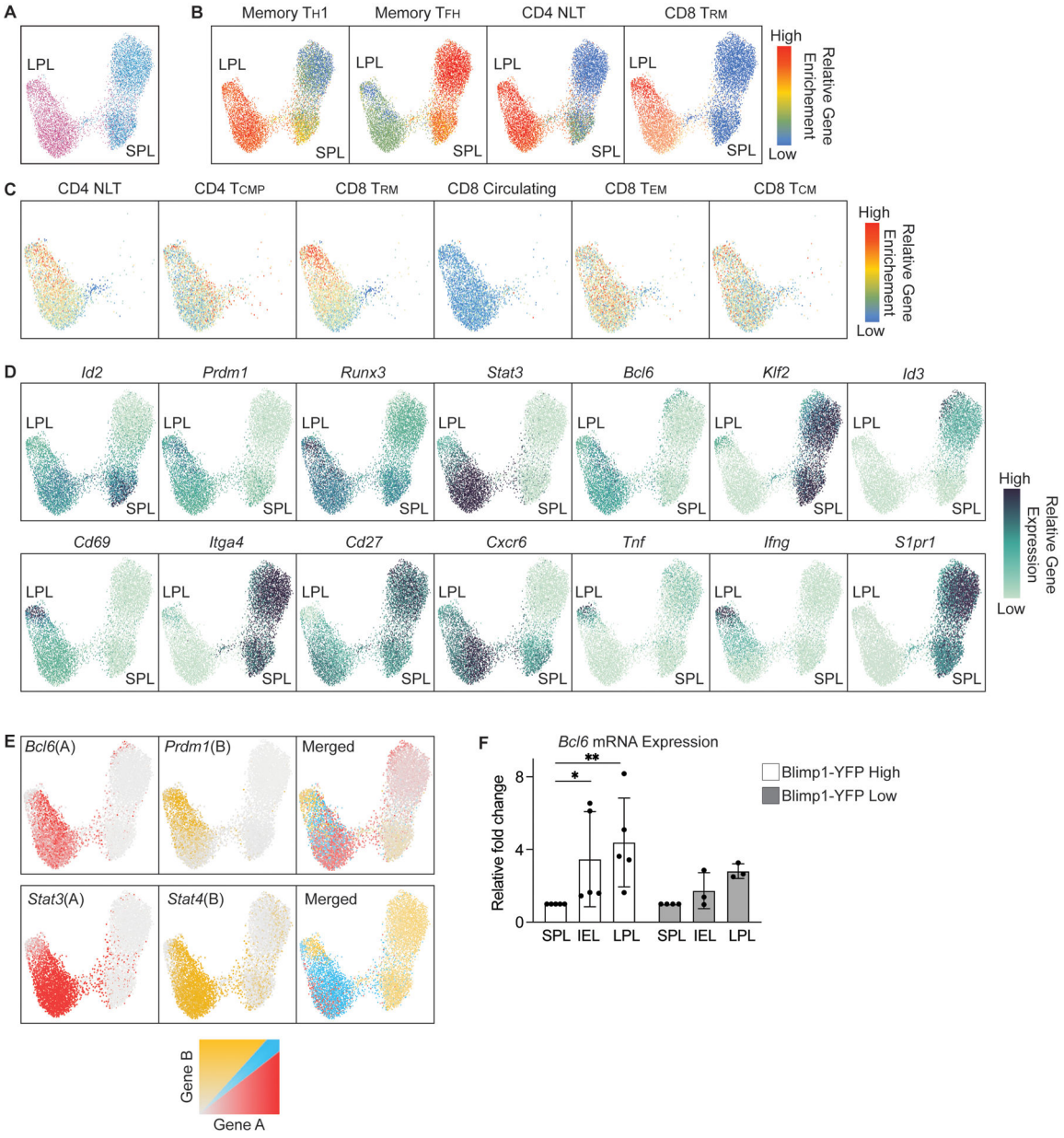

Figure 5. CD4$^+$ SI T_{RM} exhibit heterogeneity and express genes associated with both effector and memory fates.

Single-cell RNAseq of SMARTA CD4$^+$ T cells from spleen and SI on day 21 following LCMV-Arm infection. **(A)** UMAP dimensional reduction of SI and LPL SMARTA CD4$^+$ T cells colored by tissue identity. **(B-C)** UMAP reduction of SPL and LPL samples (B) or LPL samples only (C) showing relative enrichment of indicated gene signatures. **(D)** UMAP reduction showing relative expression of indicated transcriptional regulators, cell surface receptors or cytokines. **(E)** UMAP dimensional reduction showing merged expression of indicated TF pairs. **(F)** Bar plot showing relative fold-change of *Bcl6* mRNA in indicated tissue compared to spleen in Blimp1$^+$ versus Blimp1$^-$ SMARTA CD4$^+$ T cells from mice on day 15 of LCMV-Arm infection. One-way ANOVA test was performed for statistical

significance. Data are from 2 replicates (A-E) or 3 replicates (F) of cells pooled from 12–15 mice per replicate. Graphs show mean ± SD; *$p < 0.05$, ** $p<0.01$.

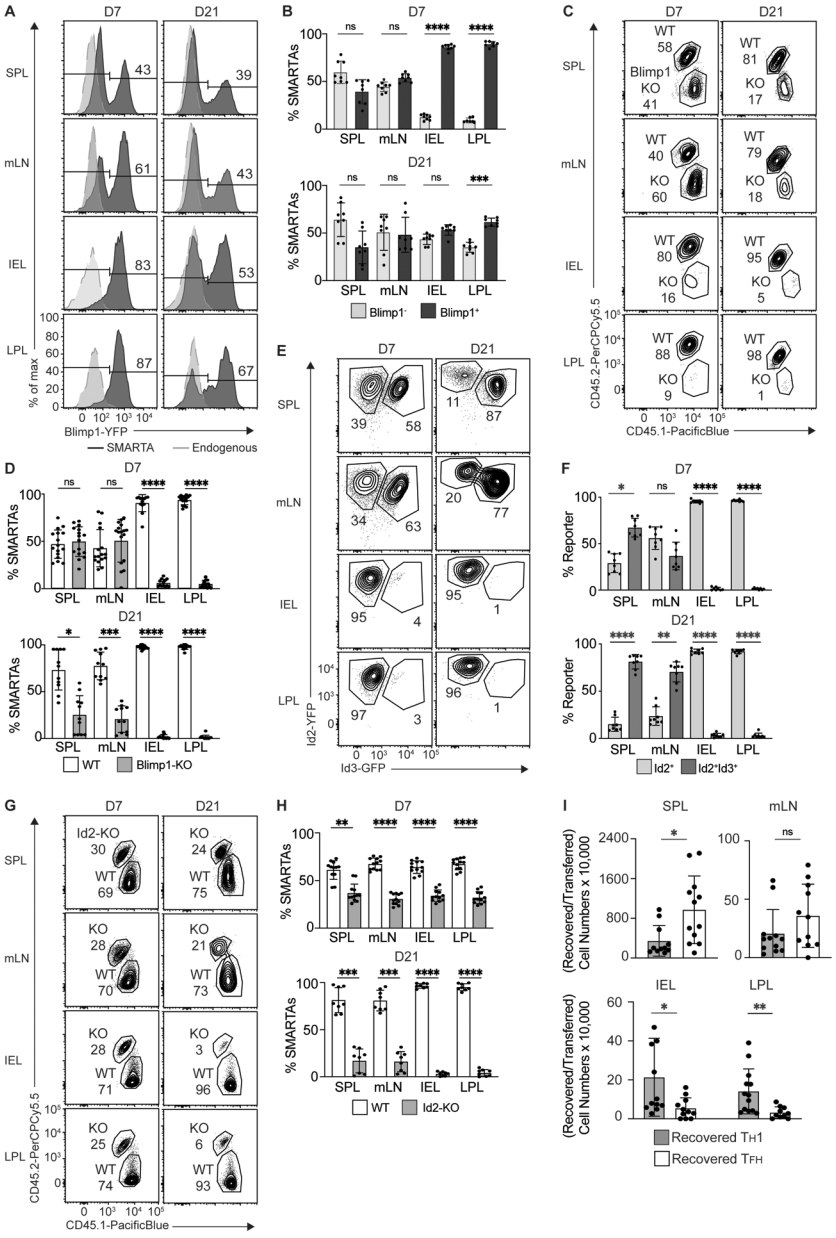

Figure 6. Loss of Blimp1 or Id2 impairs early CD4$^+$ T_{RM} differentiation.

(A) Representative histograms of Blimp1-YFP expression by SMARTA CD4$^+$ T cells from spleen, mLN, and SI on day 7 or 21 following LCMV-Arm infection. **(B)** Quantification of Blimp-YFP$^+$ cells of total SMARTA CD4$^+$ T cells in indicated tissues. **(C)** Representative flow plots showing the frequency of WT and Blimp1-KO SMARTA CD4$^+$ T cells in indicated tissues at specific time points. **(D)** Quantification of the frequency of WT and Blimp1-KO of total SMARTA CD4$^+$ T cell population. **(E)** Representative flow plots of Id2-YFP and Id3-GFP expression by SMARTA CD4$^+$ T cells from SPL, mLN, and SI on day 7 or 21 of infection. **(F)** Quantification of the frequency of Id2-YFP$^+$ or ID2-YFP$^+$Id3-GFP$^+$ cells of total SMARTA CD4$^+$ T cells. **(G)** Representative flow plots comparing the frequency of WT and Id2-KO SMARTA CD4$^+$ T cells in indicated tissues at specific

time points. **(H)** Quantification of the frequency of WT and Id2-KO of total SMARTA $CD4^+$ T cell population. Numbers in flow plots or histograms indicate percent of cells in corresponding gate. **(I)** Ratio of number of SMARTA T_H1 or T_{FH} cells recovered at day 8 of infection (day 5 post-transfer) compared to number of SMARTA T_H1 or T_{FH} cells transferred at day 6 of infection. Data are representative (A,C,E,G) or cumulative (B,D,F,H,I) of 2–4 experiments with n=2–4 mice per experiments. Graphs show mean ± SD; *p < 0.05, ** p<0.01, *** p<0.001, ****p< 0.0001. One way ANOVA (B, D, F, H) or paired t-test (I) was performed for statistical significance.

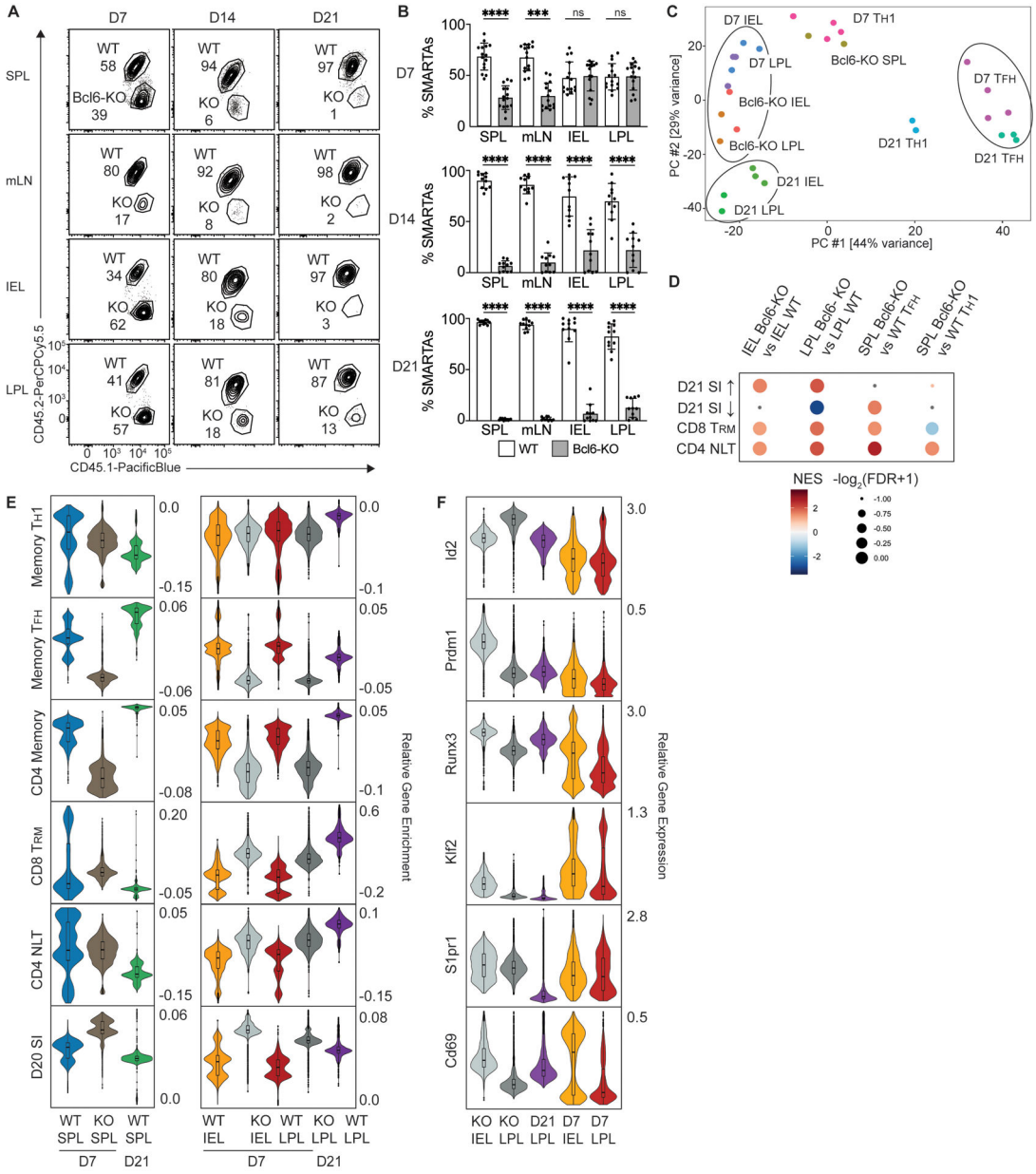

Figure 7. Loss of Bcl6 at day 7 enhances the T_{RM} differentiation program.

(A) Representative flow plots showing the frequency of WT and Bcl6-KO SMARTA $CD4^+$ T cells in indicated tissues at specific time of infection. **(B)** Quantification of the frequency of WT and Bcl6-KO of total SMARTA $CD4^+$ T cell population. **(C,D)** Bulk RNAseq of WT and Bcl6-KO SMARTA $CD4^+$ T cells from SPL and SI, harvested at day 7 of LCMV-Arm infection. **(C)** Principal component analysis (PCA) of RNAseq data. **(D)** Gene enrichment analysis (GSEA) of indicated gene signatures in day 7 RNAseq data. **(E-F)** Single-cell RNAseq analysis of WT and Bcl6-KO SMARTA $CD4^+$ T cells from SPL and SI, harvested at day 7 and 21 of LCMV-Arm infection. Violin plots showing relative enrichment of indicated gene signature (E) or relative gene expression of indicated gene (F). Data are representative (A), or cumulative (B-F) of 3 experiments with n=2–4 mice (A-B) or 2–3

replicates of cells pooled from 5–12 mice per replicate (C-F). Graphs show mean ± SD; *p < 0.05, ** p<0.01, *** p<0.001, ****p<0.0001. One way ANOVA was performed for statistical significance (B).